Cell

Mammalian Telomeres Resemble Fragile Sites and Require TRF1 for Efficient Replication

Agnel Sfeir,[1] Settapong T. Kosiyatrakul,[2] Dirk Hockemeyer,[1,3] Sheila L. MacRae,[1] Jan Karlseder,[1,4] Carl L. Schildkraut,[2] and Titia de Lange[1,*]
[1]Laboratory for Cell Biology and Genetics, The Rockefeller University, 1230 York Avenue, New York, NY 10065, USA
[2]Department of Cell Biology, Albert Einstein College of Medicine, 1300 Morris Park Avenue, Bronx, NY 10461, USA
[3]Present address: The Whitehead Institute, 9 Cambridge Center, Cambridge, MA 02142, USA
[4]Present address: The Salk Institute for Biological Studies, 10010 North Torrey Pines Road, La Jolla, CA 92037-1099, USA
*Correspondence: delange@mail.rockefeller.edu
DOI 10.1016/j.cell.2009.06.021

SUMMARY

Telomeres protect chromosome ends through the interaction of telomeric repeats with shelterin, a protein complex that represses DNA damage signaling and DNA repair reactions. The telomeric repeats are maintained by telomerase, which solves the end replication problem. We report that the TTAGGG repeat arrays of mammalian telomeres pose a challenge to the DNA replication machinery, giving rise to replication-dependent defects that resemble those of aphidicolin-induced common fragile sites. Gene deletion experiments showed that efficient duplication of telomeres requires the shelterin component TRF1. Without TRF1, telomeres activate the ATR kinase in S phase and show a fragile-site phenotype in metaphase. Single-molecule analysis of replicating telomeres showed that TRF1 promotes efficient replication of TTAGGG repeats and prevents fork stalling. Two helicases implicated in the removal of G4 DNA structures, BLM and RTEL1, were required to repress the fragile-telomere phenotype. These results identify a second telomere replication problem that is solved by the shelterin component TRF1.

INTRODUCTION

Mammalian chromosome ends feature long arrays of TTAGGG repeats that serve as binding sites for shelterin (de Lange, 2005), a telomere-specific protein complex that represses the DNA damage response. The stability of mammalian chromosomes and indeed cell viability critically depends on the maintenance of sufficient shelterin binding sites at each telomere. Telomeric DNA can be lost with cell proliferation because of the inability of the DNA replication machinery to duplicate DNA ends. This end replication problem is solved by telomerase, the reverse transcriptase that adds telomeric repeats onto the 3′ ends of chromosomes (Greider and Blackburn, 1985), thereby compensating for terminal sequence loss. Most of the long TTAGGG repeat array at the ends of mammalian chromosomes, however, is maintained by semiconservative DNA replication. Our data reveal that telomeric repeats pose a challenge to the DNA replication machinery, giving rise to replication-dependent defects that resemble those of aphidicolin-induced common fragile sites.

Fragile sites represent specific chromosomal regions that challenge replication, especially under conditions of limiting nucleotide pools or partial inhibition of DNA polymerases (Durkin and Glover, 2007). Examples are the common fragile sites, which are prone to display abnormal features in metaphase chromosomes when cells experience replication stress. Specifically, treatment with low levels of the DNA polymerase inhibitor aphidicolin induces site-specific breaks or gaps in metaphase chromosomes (Glover et al., 1984). The molecular basis of this replication dependent instability is not known. Common fragile sites are large, and sequence motifs that might explain their behavior have not been identified. The occurrence of breaks or gaps at common fragile sites is enhanced when replication stress is combined with deficiency in the ATR kinase pathway, which responds to stalled replication forks (Casper et al., 2002). Similarly, inhibition of homology-directed repair, which facilitates replication restart after replication fork collapse, exacerbates the expression of common fragile sites (Arlt et al., 2004). The idea that common fragile sites represent regions where replication forks stall and collapse is consistent with the increased rate of recombination at these loci (Feichtinger and Schmid, 1989; Glover and Stein, 1987). Indeed, common fragile sites are hotspots for deletions and other chromosome rearrangements in cancer (Yunis and Soreng, 1984; LeBeau and Rowley, 1984).

Our data identify telomeres as aphidicolin-induced fragile sites and establish that the shelterin protein TRF1 is required to prevent telomere replication problems. TRF1 is one of the six distinct proteins that make up shelterin (Chong et al., 1995; reviewed in de Lange, 2005). TRF1 and its paralogs, TRF2, bind to double-stranded TTAGGG repeats of the telomere with high fidelity. Both proteins are abundant at telomeres, binding

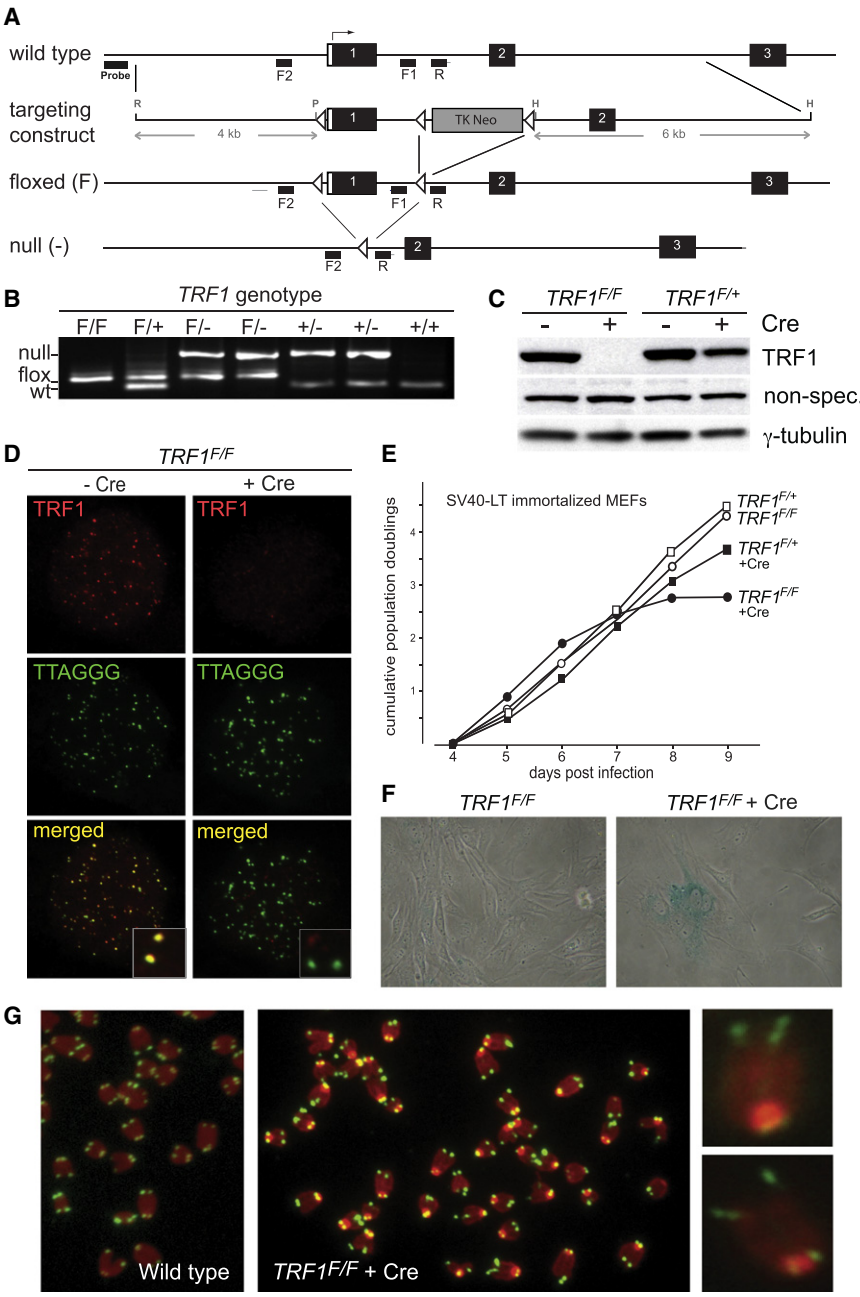

Figure 1. Conditional Deletion of Mouse *TRF1*

(A) Schematic of the mouse *TRF1* locus on chromosome 1 (NCBI locus ID 21749), the targeting construct, and the altered alleles of *TRF1*. R, EcoRI; P, PvuII; H, HindIII. F1, F2, and R, PCR primers.

(B) *TRF1* PCR on tail DNA from mice of the indicated genotypes using the F1 and F2 forward primers and the R reverse primer. PCR products: wild-type, 100 bp; flox, 152 bp; null allele, 500 bp.

(C) Immunoblot monitoring loss of TRF1 upon Cre treatment of $TRF1^{F/F}$ MEFs. TRF1 (Ab1449) was detected 3 days after Cre treatment of $TRF1^{F/F}$ and $TRF1^{F/+}$ MEFs. Cre, mock infection; γ-tubulin, loading control.

(D) IF-FISH to monitor TRF1 at telomeres of $TRF1^{F/F}$ MEFs at day 3 after Cre. TRF1 IF, red; telomeric FITC PNA probe, green.

(E) Graph representing proliferation of TRF1-deficient MEFs.

(F) Phase-contrast microscopic images of primary $TRF1^{F/F}$ MEFs before and after Cre treatment. Cells were stained for SA-β-galactosidase at day 7 after Cre.

(G) Metaphase spreads showing the fragile-telomere phenotype in TRF1 null cells. Telomeres were highlighted by FISH (green), and DNA was stained with DAPI (red) at day 4 after Cre.

throughout the telomeric DNA tract. TRF1 and TRF2 interact with TIN2, which also recruits TPP1 and POT1 to chromosome ends. POT1 also binds telomeric DNA, but unlike TRF1 and TRF2, it interacts with the single-stranded TTAGGG repeats in the 3′ overhang. TRF2 and POT1 contribute to the protection of chromosome ends by repressing DNA damage signaling by the ATM and ATR kinases, respectively (Denchi and de Lange, 2007). TRF2 and POT1 also repress the two main DNA repair pathways, nonhomologous end joining (NHEJ) and homology-directed repair (HDR) (Celli and de Lange, 2005; Celli et al., 2006; Palm et al., 2009). Although TRF1 has a similar architecture as TRF2 (Fairall et al., 2001), it has distinct domains and a different set of interacting partners (Chen et al., 2008; reviewed in Palm and de Lange, 2008). TRF1 has been shown to contribute to telomere length regulation (van Steensel and de Lange, 1997; Smogorzewska et al., 2000), but its role in telomere protection had not been established. Because TRF1 deletion in the mouse is lethal (Iwano et al., 2004; Karlseder et al., 2003), we generated a conditional allele to examine the role of TRF1 in telomere biology.

RESULTS

Conditional Deletion of TRF1

We generated a conditional allele of the mouse *TRF1* gene that allows Cre-mediated deletion of exon 1, which contains the translation start site ($TRF1^{F}$; Figures 1A and 1B). Introduction of Cre into $TRF1^{F/F}$ mouse embryo fibroblasts (MEFs) resulted in the expected loss of TRF1 protein within 72 hr (Figures 1C and 1D). Consistent with previous reports on the lethality of *TRF1* deletion (Iwano et al., 2004; Karlseder et al., 2003), loss of TRF1 induced a growth arrest and senescence in primary and SV40-LT immortalized MEFs (Figures 1E and 1F). As deletion of TRF1 was better tolerated in immortalized MEFs, they were used for these studies unless indicated otherwise. The cell-cycle arrest and other phenotypes of Cre-mediated *TRF1* deletion were suppressed by exogenous TRF1 (Figure S1 available online, and

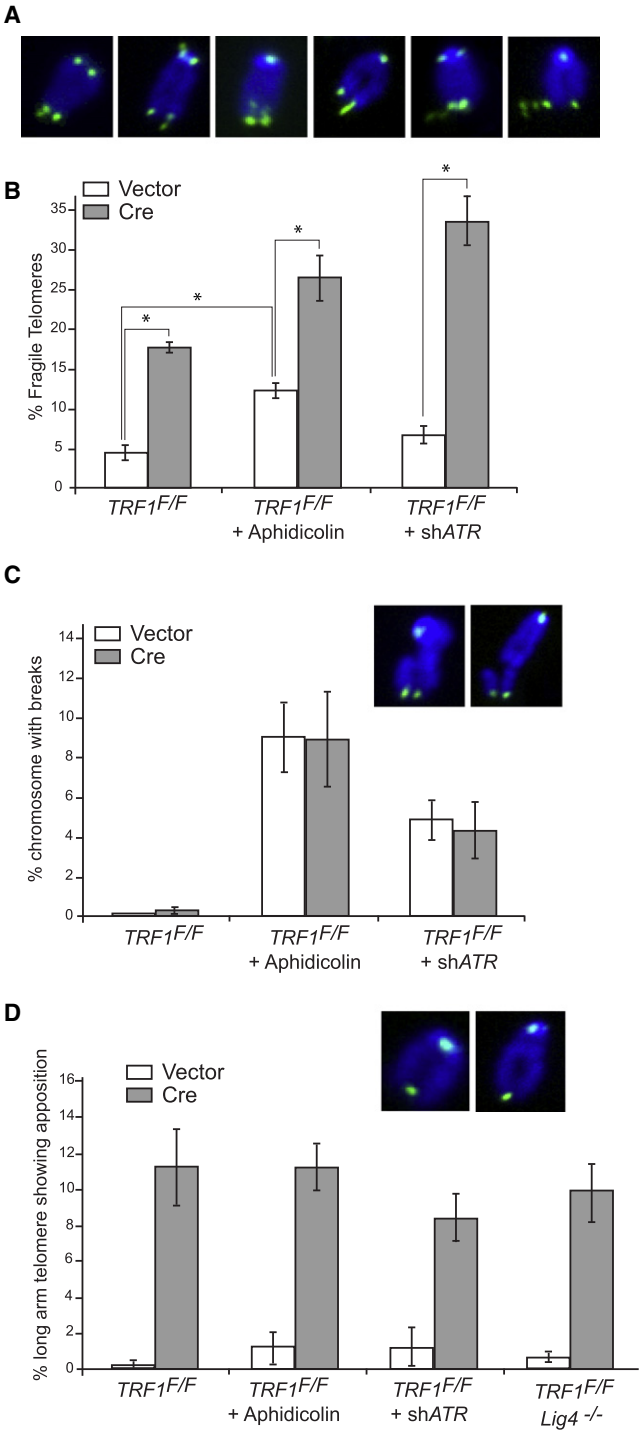

Figure 2. Effects of TRF1, Aphidicolin, and ATR shRNA

(A) Examples of the fragile telomeres in *TRF1*$^{F/F}$ MEF metaphases at day 4 after Cre. Telomeric DNA, FITC PNA probe (green); DNA, DAPI (blue).

(B) Quantification of fragile telomeres induced by deletion of TRF1 with or without treatment with 0.2 μM aphidicolin or ATR shRNA. Bars represent mean values of three independent experiments with SDs. Asterisks, $p < 0.01$ based on a two-tailed Student's t test.

(C) Quantification of chromosome breaks/gaps. Experimental conditions are as in (B).

(D) Quantification of long arms telomere associations in response to the indicated treatments. Experimental conditions are as in (B). Sister telomere associations were only scored on long arms. Sister associations were significantly reduced ($p < 0.05$ based on a two-tailed Student's t test) by treatment of TRF1 null cells with ATR shRNA but not by aphidicolin treatment or absence of DNA ligase IV (lig4$^{-/-}$).

see below), demonstrating that they are indeed a consequence of TRF1 loss.

TRF1-deficient cells did not show a strong telomere fusion phenotype, as fewer than 2% of the metaphase chromosomes became joined and genomic DNA analysis showed that both the telomeric restriction fragment lengths and the telomeric 3′ overhang were unaltered (Figures S2A and S2B). These results contrast the phenotype of TRF2 deletion, which induces telomere fusions and a concomitant loss of the 3′ overhang (Celli and de Lange, 2005). Deletion of TRF1 also did not lead to the strong increase in telomeric overhang signals observed upon deletion of POT1b, nor did the cells show the endoreduplication phenotype associated with the loss of POT1a (Figures S2B and S2C) (Hockemeyer et al., 2006). Furthermore, TRF1 deletion did not change the expression levels of Rap1, POT1a, or TRF2 (Figures S2D and S2E and data not shown), and there were only moderate effects on the association of Rap1, TRF2, TPP1, and POT1a with telomeric DNA as measured by ChIP (Figure S2F).

TRF1 Deletion Results in Aberrant Telomeres in Metaphase

The most notable phenotype of TRF1 deletion was a high incidence of telomeres with an aberrant structure in metaphase (Figures 1G and 2A). The telomeric FISH signal at individual chromatid ends is normally represented as a single signal with an intensity that is roughly equal to the telomeric signal of the sister chromatid end. After TRF1 deletion, a large fraction of chromatids had multiple telomeric signals (Figures 2A and 2B). In some cases, the multiple signals were spatially separated from the chromatid end, as if the telomeric DNA had failed to condense or was broken. We refer to these various abnormal telomeric patterns as fragile telomeres.

Up to 20% of the telomeres showed this aberrant structure in TRF1 null cells, whereas fragile telomeres were less frequent (<5%) in control cells (Figure 2B). Chromosome-orientation FISH (CO-FISH) showed that both sister telomeres were roughly equally prone to display the fragile phenotype (Figure S3A and data not shown). Aberrant telomeric structures (often referred to as telomere doublets) resembling the fragile telomeres documented here were previously reported in several settings, including embryonic stem cells (ESCs) lacking TRF1 (Philippe et al., 1999; Undarmaa et al., 2004; Iwano et al., 2004; van Overbeek and de Lange, 2006; Blanco et al., 2007; Okamoto et al., 2008), but the underlying telomeric defect had not been identified.

In addition to the fragile telomeres, we observed frequent associations of sister telomeres in TRF1 null cells (Figure 2D). These telomere associations did not result from NHEJ since they also occurred upon deletion of TRF1 from cells lacking DNA ligase IV (Figure 2D). The molecular nature of these associations remains to be determined, but, given the data presented

below, it is tempting to speculate that the sister telomere associations represent the recently described sister chromatid bridges at fragile sites (Chan et al., 2009).

Fragile Telomeres Are Induced by Aphidicolin and Respond to Inhibition of ATR

In order to test whether the fragile-telomere phenotype resembles that of the common fragile sites, we examined metaphases of wild-type MEFs treated with low concentrations of aphidicolin (0.2 μM). Consistent with previous data (Glover et al., 1984), aphidicolin induced breaks in ~8% of chromosomes (Figures 2C, S3B, and S3C). Importantly, aphidicolin induced a striking increase in the frequency of fragile telomeres (Figure 2B). The effect of aphidicolin was additive with deletion of TRF1, resulting in ~28% of telomeres showing this phenotype (Figure 2B). Aphidicolin did not affect the sister telomere associations seen after TRF1 deletion (Figure 2D).

In order to determine the effect of ATR on the fragile-telomere phenotype, *TRF1*$^{F/F}$ MEFs were treated with Cre and subsequently with ATR short hairpin RNA (shRNA) (Figure S3D). As for the common fragile sites (Casper et al., 2002), ATR inhibition strongly enhanced the fragile-telomere phenotype of TRF1-deficient cells (Figures 2B and S3B–S3E). In contrast, inhibition of ATR did not increase the sister telomere association phenotype of TRF1 null cells (Figure 2D). Collectively, the data obtained with cells treated with aphidicolin or ATR shRNA demonstrate that telomeres resemble common fragile sites and that this feature of telomeres is partially repressed by TRF1.

S Phase-Dependent ATR Signaling upon Loss of TRF1

Consistent with a DNA replication defect, cells lacking TRF1 showed a strong telomere damage response phenotype, as evidenced by 53BP1 and γ-H2AX telomere dysfunction-induced foci (TIFs) (Takai et al., 2003) (Figures 3A, 3B, and S4). The TIF response was fully repressed by exogenous TRF1, establishing that it was due to TRF1 loss (Figure S1). Using MEFs with compound genotypes, we determined whether this DNA damage signal depended on the ATM, DNA-PKcs, or ATR kinase. Of these three kinases, only ATR was required for the TIF response (Figures 3A, 3B, and S5). Consistent with ATR signaling, Chk1 became phosphorylated upon deletion of TRF1, whereas phosphorylation of the ATM target Chk2 was not detected (Figures 3C and 3D).

We next asked whether progression through S phase was required for the activation of ATR at telomeres lacking TRF1. To test this, we deleted TRF1 from quiescent (G_0) primary *TRF1*$^{F/-}$ cells. As a positive control, TRF2, which is known to be required for telomere protection in all stages of the cell cycle (Konishi and de Lange, 2008), was deleted from a parallel culture of quiescent primary *TRF2*$^{F/-}$ cells. While deletion of TRF2 resulted in the expected 53BP1 foci at telomeres, the TIF response was minimal in G_0 cells lacking TRF1 (Figures 3A, 3B, and S5). TIFs only became prominent when the cells were released from G_0 and progressed through S phase (Figures 3E and S5). These results demonstrate that progression through S phase in absence of TRF1 induces an ATR-dependent DNA damage signal at telomeres. As most cells in an asynchronous population of immortalized TRF1 null cells showed numerous TIFs, it is likely that much of the DNA damage generated at telomeres in S phase persists when TRF1 is absent.

Analysis of Telomere Replication in Wild-Type Cells using SMARD

We used SMARD (single-molecule analysis of replicated DNA; Norio and Schildkraut [2001]) to examine the progression of replication forks through telomeric DNA (Figure 4A). SMARD relies on two sequential periods of in vivo labeling with different halogenated nucleotides (IdU and CldU) to mark replicating DNA molecules. Genomic DNA from the labeled cells was digested with frequently cutting restriction enzymes that cleave most of the genomic DNA into small fragments but do not cut in the long (>20 kb) TTAGGG repeat arrays, so that DNA fragments with a molecular weight (MW) >25 kb isolated from an agarose gel were enriched for telomeric DNA. The incorporation of IdU and CldU was visualized with fluorescent antibodies in partially denatured DNA molecules stretched onto silanized glass slides. We identified the telomeric DNA fragments with a FISH-PNA probe (TelC) that anneals to the G-rich telomeric repeat strand. Although annealing of the TelC probe interferes with detection of the IdU and CldU in the TTAGGG repeats, substitutions in the CCCTAA repeat strand are detectable. Both the telomeric FISH signal and the IdU or CldU fluorescent signals appeared as strings of dots that were often interrupted due to the partial denaturation of the DNA (Figure 4A). Nonetheless, long telomeric DNA molecules were readily identified among the mixture of DNA fragments. The optimized procedure used pulse-labeling periods of 30 min followed by a 3 hr chase. Since this procedure only labels the DNA in cells that are in S phase during the pulses, the protocol was further improved by repeating the pulse-chase six times. The total duration of the six rounds of pulse/chase was 21 hr, which is less than the cell doubling time. As replication forks progress at ~2 kb/min (Anglana et al., 2003), even the longest telomeres (~150 kb) should be fully replicated within one round of the double-pulse/chase procedure. As expected, the average length of the IdU and CldU segments was approximately equal, and the two substitutions were observed in approximately equal fractions of the telomeric DNA molecules. Because the telomeric DNA fragments used for the analysis are of variable lengths, the rate of fork progression cannot be determined accurately in these experiments. However, given that we frequently observed telomeric fragments in the >25 kb size range that were completely labeled with either IdU or CldU in experiments using 30 min pulses, it is unlikely that the fork rate is lower than 1 kb/min.

The final protocol yielded telomeric DNA molecules with a pattern of IdU/CldU incorporation that could be consistent with replication proceeding from a subtelomeric origin toward the chromosome end (Figure 4A). To determine the direction of the replication fork, we analyzed telomeric DNA molecules with an attached segment of subtelomeric DNA generated by digestion with SwaI (Figure 4B). The length of the telomeric SwaI fragments is ~180 kb as identified by genomic blotting (see inset in Figure 4B). In this size fraction of SwaI-digested DNA, the telomeric fragments are not strongly enriched, limiting the number of telomeric molecules available for analysis. Nonetheless, we identified 90 telomeric SwaI restriction fragments, which had

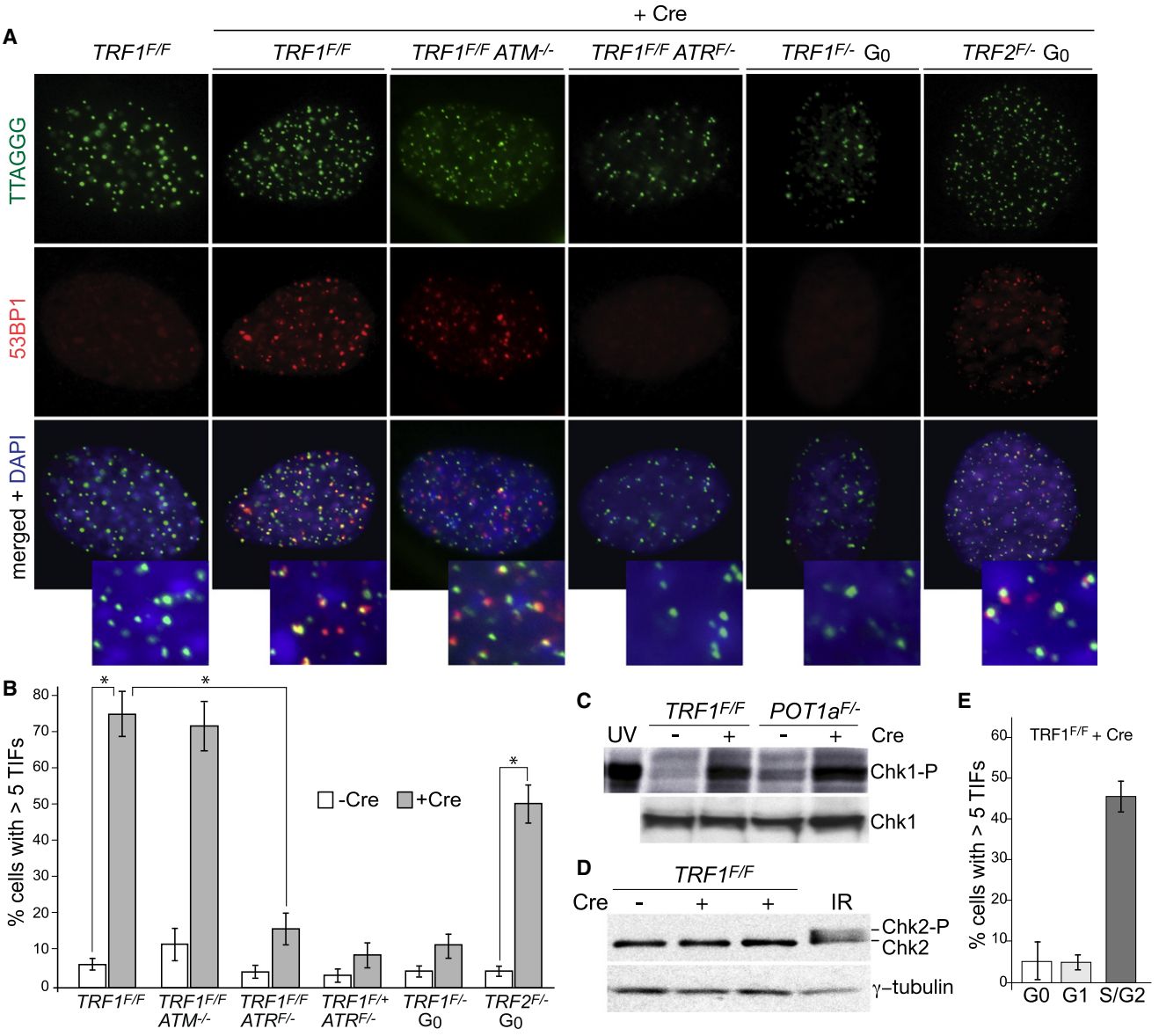

Figure 3. Deletion of TRF1 Results in an S Phase-Dependent ATR Kinase Signal

(A) ATR-dependent TIF formation upon deletion of TRF1 from cycling cells. Cells with the indicated genotypes were analyzed at day 4 after pWZL-Cre using FISH for telomeres (green), IF for 53BP1 (red), and DAPI DNA counterstain (blue). So that the lethality associated with ATR deletion could be circumvented, the *TRF1*$^{F/F}$ *ATR*$^{F/F}$ cells were arrested in G_0 by contact inhibition and serum starvation, infected with Ad-Cre, released at day 3, and analyzed 1 day later. For the two right-hand panels, *TRF1*$^{F/-}$ and *TRF2*$^{F/-}$ cells were similarly arrested in G_0 and infected with Ad-Cre, but were analyzed at 4 day while in G_0. Deletion of ATR, TRF1, and TRF2 was verified by immunoblotting (Figure S5).

(B) Quantification of the TIF response as shown in (A). Bargraphs represent mean values of three independent experiments and SDs. Asterisks, $p < 0.01$ based on a two-tailed Student's t test.

(C) Immunoblot for Chk1 phosphorylation. Cells with the indicated genotypes were analyzed at day 6 after Cre. POT1a null MEFs and cells treated with UV (25 J/m^2, 30 min recovery) serve as positive controls.

(D) Immunoblot for Chk2 phosphorylation. Cells were treated as in (C). MEFs treated with IR (2 Gy,1 hr recovery) serve as a positive control.

(E) S phase-dependent induction of TIFs. *TRF1*$^{F/F}$ cells were synchronized in G_0 and infected with Ad-Cre and analyzed as in (A). For G_1, cells were released into normal medium on day 3 after Cre and harvested 15 hr after release. S/G2 cells were released into normal medium followed by an aphidicolin block and analyzed 7 hr after release from the G1/S block. Bar graphs represent mean values of three independent experiments and SDs. TRF1 was deleted in ~50% of the cells (Figure S5). FACS analysis of the G_0, G1, and S/G2 cells is shown in Figure S5.

a labeled (IdU or CldU) segment that extended beyond the telomeric DNA labeled with FISH (Figure 4B). The presence of IdU or CldU in the subtelomeric segment and the absence of substitution in the distal end of the molecules is consistent with progression of the replication fork from a subtelomeric site into the telomeric DNA. We also observed molecules with IdU in the

subtelomeric segment that contained IdU at the proximal end and CldU at the distal end. Again, this configuration is consistent with replication from a subtelomeric origin.

Occasional Replication Initiation within Telomeric Repeats in Wild-Type Cells

We observed a small number of telomeric DNAs that suggested initiation of DNA replication within the telomeric repeats (Figure 4C). These molecules contained an IdU segment flanked on both sides by segments of CldU, indicating that replication had started in the telomeric sequences during the IdU pulse and continued in both directions during the CldU pulse. In some cases, replication proceeded both from a subtelomeric origin and an origin within the telomere, leading to convergence of two forks within the telomeric repeats. The frequency of initiation events within the telomeric DNA was low; only ~3% of telomeric molecules showed a pattern consistent this mode of replication. Occasional initiation of DNA replication in the telomeric repeat array is consistent with the relative lack of sequence specificity of mammalian ORC (Falaschi et al., 2007). In addition, the association of ORC components with shelterin (Deng et al., 2007; Tatsumi et al., 2008; Atanasiu et al., 2006) could contribute to formation of a prereplication complex within the telomeric DNA.

Diminished Telomeric Replication upon Deletion of TRF1

To determine whether TRF1 affected the efficiency of telomere replication, we measured the fraction of telomeric DNA molecules that contained either IdU or CldU (or both) in DNA obtained from TRF1-proficient and -deficient cells (Figure 5). In three independent experiments, the deletion of TRF1 resulted in an ~2-fold lower incorporation of halogenated nucleotides in telomeric DNA molecules regardless of their length. This effect was not due to a general reduction in DNA replication since the incorporation of BrdU was not altered at the time point studied (Figure S2C). As a control, the well-studied replicating region derived from the Igh locus (Norio et al., 2005) was unaffected by deletion of TRF1 (Figure 5). Thus, deletion of TRF1 had a specific effect on the replication of telomeric DNA. Furthermore, the efficiency of telomere replication was not altered when TRF2 was deleted from *TRF2*$^{F/-}$ *Lig4*$^{-/-}$ MEFs (Figure 5), and deletion of TRF2 did not induce a fragile-telomere phenotype (Celli and de Lange, 2005), indicating a specific role for TRF1 in facilitating telomere replication.

Evidence for Replication Fork Stalling

Inspection of SwaI-digested telomeric DNA molecules, which carry a subtelomeric DNA segment, revealed several cases of IdU/CldU-labeling patterns consistent with replication fork stalling in or before the telomeric DNA (Figure 6A). Among 97 telomeric molecules from TRF1-deficient cells, seven showed IdU or CldU incorporation in the subtelomeric DNA but no incorporation in the telomeric segment. These patterns would indicate that in the absence of TRF1, the fork has a greater tendency to stall when it encounters telomeric DNA. Such molecules were not identified among 78 telomeric SwaI fragments that were derived in a parallel experiment with TRF1-proficient cells.

Additional evidence for fork stalling was obtained from the occasional molecules generated by replication initiation within the telomeric repeats. We observed telomeric DNA molecules with a nonterminal IdU segment that was short compared to other molecules in the same experiment, indicative of initiation of replication in the telomeric DNA at the end of the IdU pulse (Figure 6B). In these molecules, the IdU segment is flanked on one side by CldU, indicating fork progression during the CldU-labeling period. Importantly, a significant number of these molecules showed no CldU incorporation at the other side of the IdU segment, indicating that the fork on that side did not progress during the CldU-labeling period. Although the number of this type of replication products was small (14 out of 250 IdU- and/or CldU-labeled molecules), they were never observed in DNA from TRF1-proficient cells processed in parallel (400 IdU- and/or CldU-labeled molecules examined), demonstrating again that absence of TRF1 impairs the normal progression of the replication fork.

Fragile Telomeres in Human Cells

We next asked whether human telomeres also resemble fragile sites. Since it is difficult to fully inactivate human TRF1 with RNA interference (RNAi) or dominant-negative alleles, we determined whether treatment of human cells with aphidicolin induced the fragile-telomere phenotype. Using the same low level of aphidicolin applied to mouse cells, we observed an increase in the frequency of fragile telomeres as compared to untreated cells (Figure S7A). Thus, it is likely that human and mouse telomeres are similar with regard to posing a challenge to the replication fork.

Effect on Telomere Maintenance

We considered the possibility that the fragile-telomere phenotype might lead to loss of telomeric DNA. TRF1 null cells contained a small fraction of chromosome ends that appeared to lack telomeric signals, and this phenotype was somewhat stronger when ATR was inhibited (Figure S2A). However, the length of the telomeric restriction fragments of TRF1 null cells was unaltered (Figure S2B). Because small telomere length changes are difficult to detect in mouse cells, we addressed the question of potential telomeric DNA loss in the human fibrosarcoma clone HTC75. We followed the effect of aphidicolin on telomere length in HTC75 cells over 50 population doublings (Figure S7C). As a control, parallel cultures were treated with a concentration of zeocin that induced approximately the same number of DNA damage foci per cell (Figure S7D). Neither zeocin nor aphidicolin induced loss of the telomeric DNA in HTC75 cells. Rather, aphidicolin, but not zeocin, resulted in moderate telomere elongation (Figure S7B). Thus, the replication problems in telomeres are not a major source of telomere loss in telomerase-positive cells, and they may even enhance the telomerase pathway. In budding yeast, partial inhibition of DNA replication also induces telomere elongation (Carson and Hartwell, 1985; Adams and Holm, 1996).

The Mechanism by which TRF1 Represses Telomere Fragility

As deletion of TRF1 but not TRF2 affected telomere replication, we asked whether a specific feature of TRF1 was responsible for

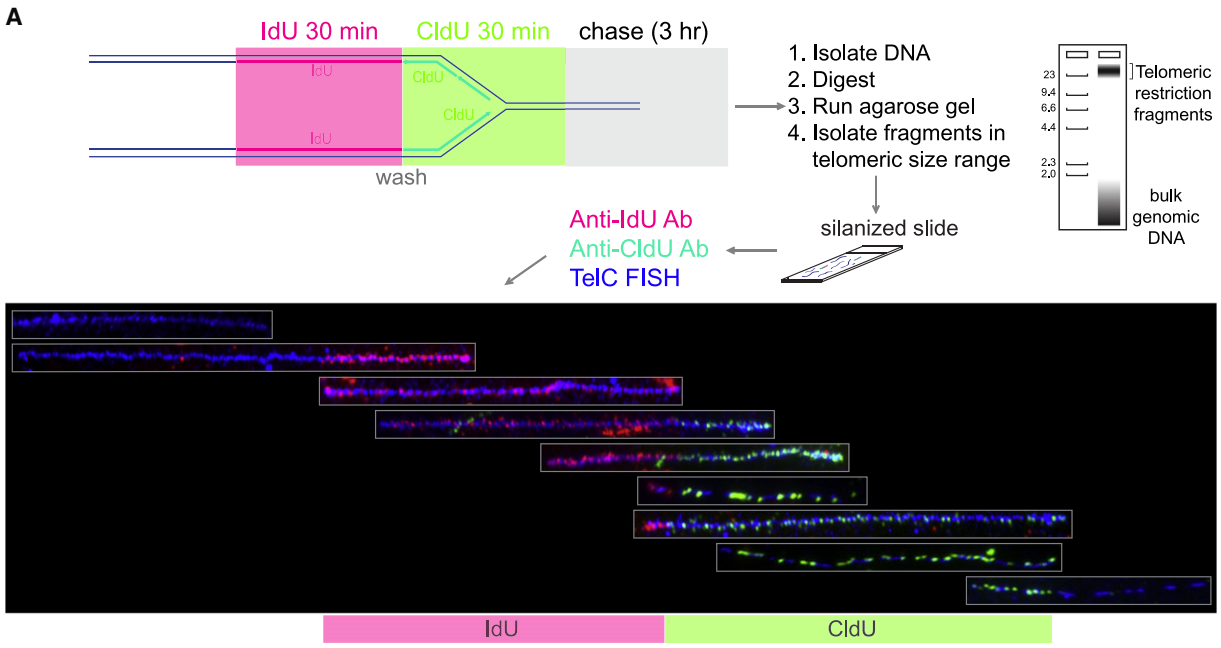
A
IdU 30 min
CldU 30 min
chase (3 hr)
IdU
CldU
CldU
IdU
wash
1. Isolate DNA
2. Digest
3. Run agarose gel
4. Isolate fragments in telomeric size range
23
9.4
6.6
4.4
2.3
2.0
Telomeric restriction fragments
bulk genomic DNA
silanized slide
Anti-IdU Ab
Anti-CldU Ab
TelC FISH
IdU
CldU

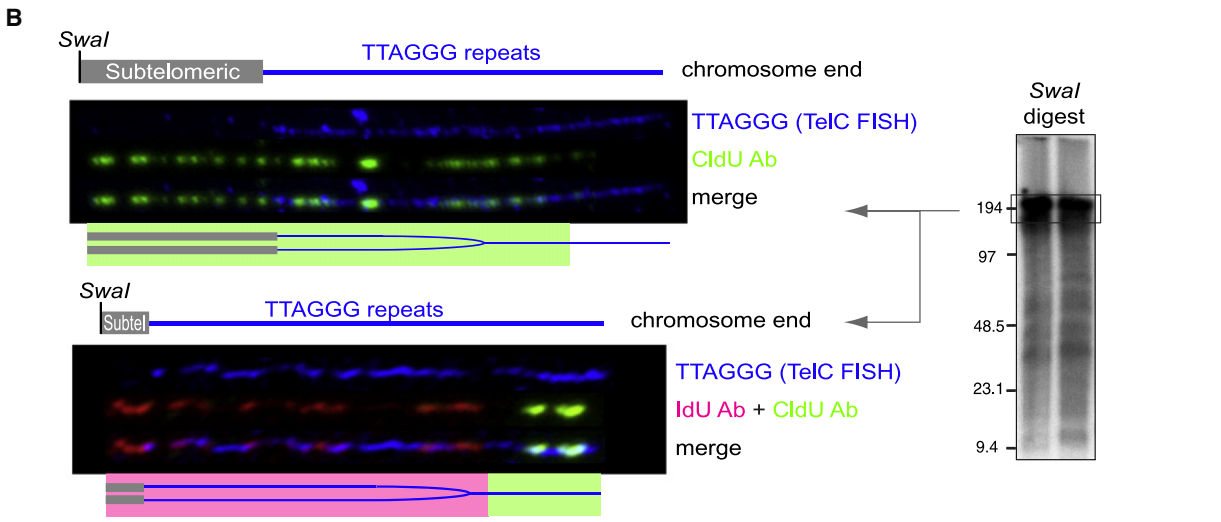
B
SwaI
Subtelomeric
TTAGGG repeats
chromosome end
TTAGGG (TelC FISH)
CldU Ab
merge
SwaI
digest
194
97
48.5
23.1
9.4
SwaI
SubtelI
TTAGGG repeats
chromosome end
TTAGGG (TelC FISH)
IdU Ab + CldU Ab
merge

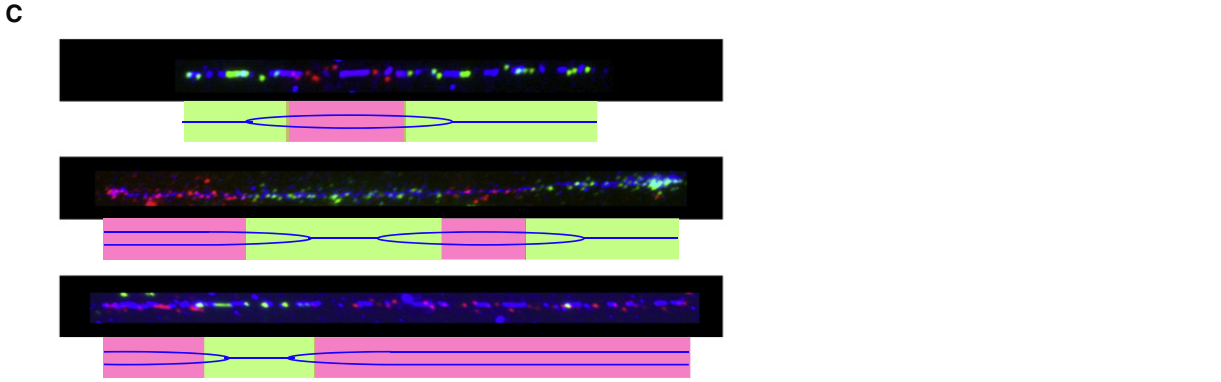
C

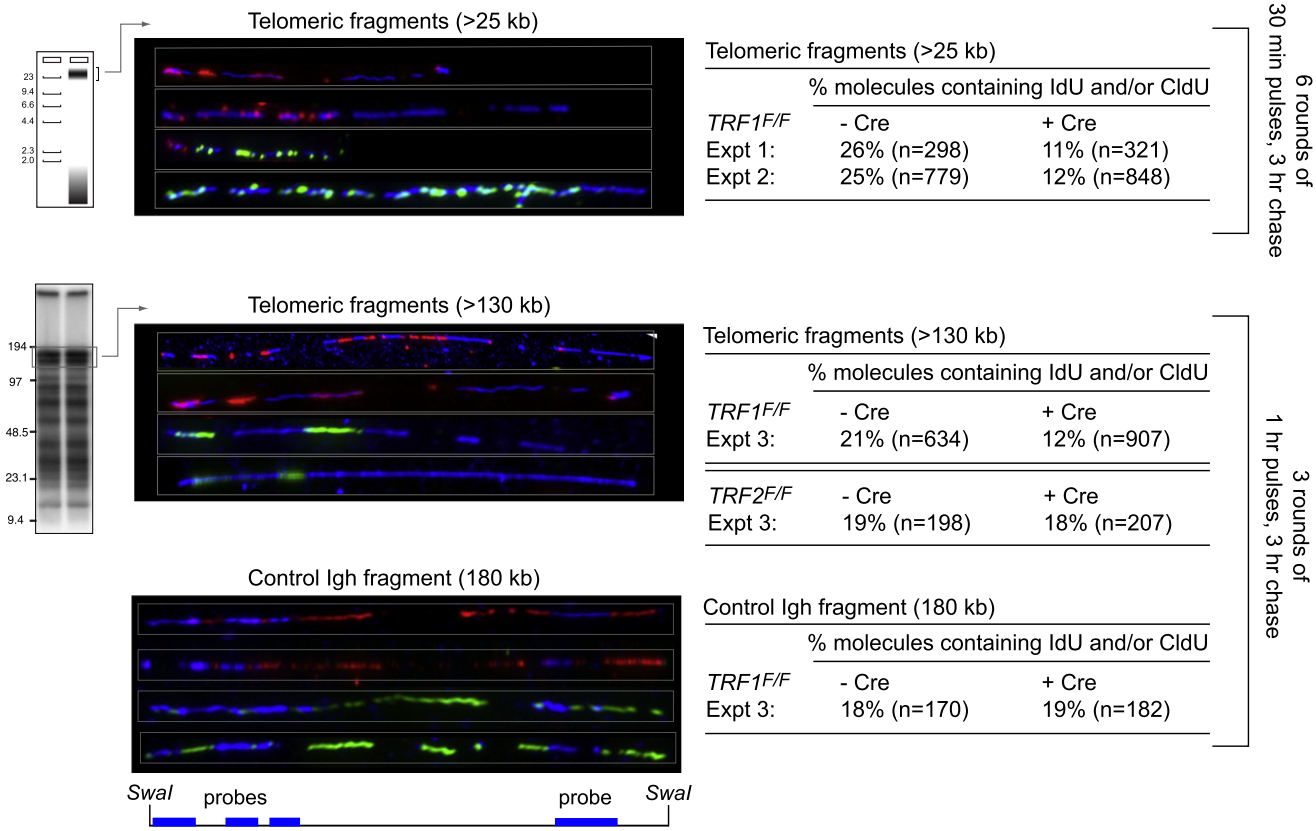

Figure 5. Deletion of TRF1 Diminishes the Replication Efficiency of Telomeric DNA

SMARD assay results from three independent experiments in which TRF1 was deleted from *TRF1*$^{F/F}$ MEFs. Cells were labeled with IdU and CldU as indicated on the right at day 4 after infection with H&R Cre retrovirus (+Cre) or vector control (−Cre). In the upper panel (experiments 1 and 2), DNA was digested with frequently cutting enzymes, and telomeric restriction fragments >25 kb were isolated (schematic on the left). Telomeric DNA molecules were identified by FISH, and the percent of molecules containing IdU and/or CldU was determined. In the middle panel, telomeric MboI/AluI fragments in the 130–180 kb range (see genomic blot inset) were isolated from a CHEF gel, and the fraction of telomeric molecules that contained IdU and/or CldU was determined as above. SMARD assay was done in one experiment in which TRF2 was deleted from *TRF2*$^{F/F}$ *DNA-Lig4*$^{-/-}$ cells and the fraction IdU- and/or CldU-labeled telomeric molecules (130–180 kb range) was analyzed. In the lower panel, the DNA preparation of *TRF1*$^{F/F}$ MEFs used in the middle panel was digested with SwaI and a 180 kb restriction fragment from the Igh locus was isolated. DNA probes from that locus (see map below) were used to identify the Igh fragments on stretched DNA, and the ratio of labeled versus unlabeled fragments was determined.

its function. Although TRF1 is notably different from TRF2 in its N-terminal domain, which is acidic, this domain was not responsible for the repression of replication problems. TRF1$^{\Delta Ac}$ fully repressed the fragile-telomere phenotype of TRF1 null cells, whereas TRF1$^{\Delta Myb}$, which lacks the ability to bind to telomeric DNA, was unable to complement the loss of the endogenous TRF1 (Figures 7A and 7B). The repression of replication problems was also not due to a change in TERRA, a class of RNA polymerase II transcripts that contain UUAGGG repeats (Azzalin et al., 2007). Although TRF1 was shown to be in a complex with RNA polymerase II, and was suggested to contribute to TERRA metabolism (Schoeftner and Blasco, 2008), no change in the abundance of TERRA was observed in TRF1 null cells (Figure 7B).

We next considered that TRF1 might repress replication problems by recruiting a class of helicases that can remove G4 DNA

Figure 4. SMARD Analysis of Telomere Replication in Wild-Type Cells

(A) Top: schematic depiction of the SMARD protocol to visualize the replication of single telomeric DNA molecules. See text for description. Bottom: telomeric DNA molecules of variable lengths identified by telomeric FISH (TelC; blue) with incorporated IdU and CldU detected with fluorescent antibodies (red and green, respectively). The telomeric fragments are organized assuming that replication proceeds from a subtelomeric origin toward the chromosome end.

(B) Two examples of replication fork progression toward the chromosome end. SMARD on ~180 kb telomeric DNA SwaI fragments containing subtelomeric DNA of variable lengths. The procedure was as in (A), except that the DNA was digested with SwaI and resolved on a pulse-field gel (see genomic blot inset). Duration of the IdU and CldU pulses was 1 hr each. The pattern is consistent with replication forks progressing from a subtelomeric origin toward the chromosome end, as depicted in the cartoon below each SMARD image.

(C) Examples of three telomeric molecules with IdU/CldU incorporation patterns consistent with replication initiating in the TTAGGG sequence. The procedure was as in (A).

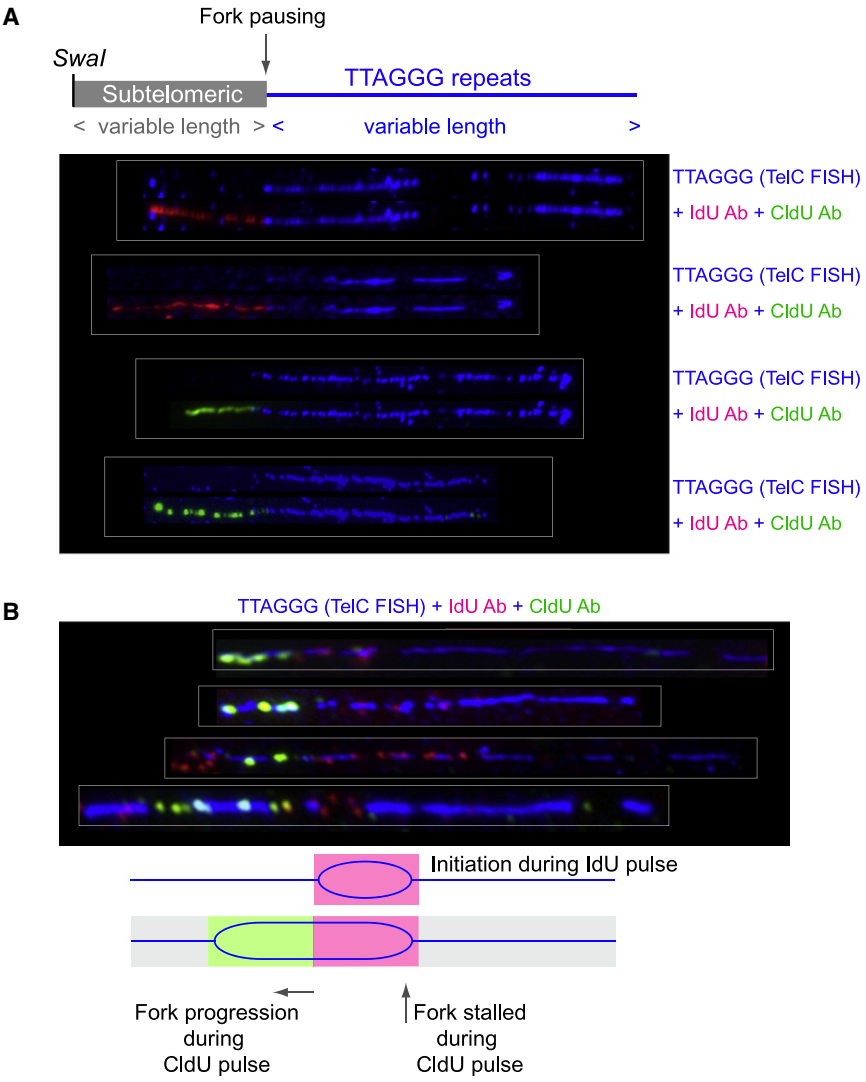

Figure 6. Evidence for Fork Stalling at Telomeres in Cells Lacking TRF1

(A) Evidence for replication fork stalling at the subtelomeric/telomeric boundary. Shown are four SwaI DNA fragments containing telomeric repeats and subtelomeric DNA from cells lacking TRF1. For the procedure, see Figure 4. Molecules shown represent incorporation patterns of IdU and CldU consistent with replication of the subtelomeric DNA (lacking TelC FISH signal) and fork stalling at the boundary of subtelomeric and telomeric DNA as shown in the schematic.

(B) Evidence for replication fork stalling after initiation of DNA replication within telomeric DNA in TRF1-deficient cells. DNA was cut with frequently cutting restriction enzymes and molecules >25 kb were isolated. Labeling was performed as in Figure 5, top panel. The patterns of incorporation of IdU and CldU are consistent with initiation of replication within the telomeric DNA near the end of an IdU pulse followed by fork progression in only one direction during the CldU-labeling period.

structures. G4 DNA can be formed by single-stranded TTAGGG repeats and might impede the replication fork. One candidate helicase is the BLM RecQ helicase, which contains the FxLxP TRF1 binding motif (FILMP at aa 311 of human BLM), binds TRF1 in vitro (Lillard-Wetherell et al., 2004), and binds and unwinds G4 DNA (Sun et al., 1998; Huber et al., 2002; Huber et al., 2006). Indeed, BLM-deficient mouse cells (Luo et al., 2000) showed a high frequency of spontaneous fragile telomeres (Figure 7C), whereas cells lacking another RecQ helicase, WRN, did not show this phenotype. Furthermore, a BLM shRNA induced the fragile-telomere phenotype, and this effect appeared to be epistatic with TRF1 (Figures 7D and 7E). A second candidate helicase that has been proposed to act on G-rich telomeric DNA is RTEL1, which affects telomere length setting in mouse species (Ding et al., 2004) and was recently shown to be functionally similar to Srs2, a budding yeast helicase that inhibit the Rad51 HDR pathway (Barber et al., 2008). Interestingly, the published metaphases of RTEL1-deficient ESCs show a mild fragile-telomere phenotype, although the frequency of this phenotype was not reported (Ding et al., 2004). RTEL1 shRNA induced fragile telomeres, and, as was the case with BLM, this phenotype appeared epistatic with deletion of TRF1 (Figures 7D and 7E). It will be necessary to derive *Blm/TRF1* DKO and *Rtel1/TRF1* DKO cells to further corroborate that TRF1 acts by recruiting/activating these helicases to telomeres.

DISCUSSION

Mammals employ TTAGGG repeats to mark the ends of their chromosomes. These repeats have been used to protect chromosome ends throughout eukaryotic evolution and remain the predominant telomeric repeat in most eukaryotic phyla. Despite the obvious utility of this sequence, there is a potential drawback of the TTAGGG repeat-based telomere protection strategy, which we report on here. Our data establish that the telomeric regions of mouse and human chromosomes challenge DNA replication, leading to a phenotype resembling common fragile sites.

Telomeres as Fragile Sites

Telomeres were not previously recognized as fragile sites, most likely because their terminal position prohibits the observation of the DNA distal to the gaps and breaks, unless the telomeric DNA is highlighted by FISH. Telomeric FISH showed that telomeres can attain a variety of aberrant structures, ranging from a simple gap to long strings of fragmented telomeric signals or even an extended strand of telomeric DNA. These cytological aspects of the fragile-telomere phenotype are informative because they provide direct observation of the aberrant structure. In contrast, FISH probes that mark the center of instability of the very large common fragile sites often do not coincide with the actual breaks or gaps, which can occur at a distance (Becker et al., 2002).

Since the structure of the fragile telomeres is highly varied, it is unlikely that the underlying lesion is a simple double-stranded DNA break. Our observations are more compatible with altered packaging and/or condensation of the chromatin perhaps due to extended areas of single-stranded DNA resulting from incomplete replication or processing of stalled forks.

The Origin of the Telomere Replication Problem

It will be important to determine what aspect of the telomeric DNA is causing problems during DNA replication. The fragile-telomere phenotype is not a consequence of late replication as mammalian telomeres replicate throughout S phase (Ten Hagen et al., 1990; Wright et al., 1999). We also consider it unlikely that the terminal position of the TTAGGG repeats is responsible for the fragile nature. First, it is clear from our data that fork arrest is occurring at a substantial distance from the actual chromosome end. Furthermore, an aphidicolin-induced fragile site in Chinese hamster chromosomes is at or near interstitial telomeric DNA (Musio et al., 1996), suggesting that internally placed telomeric repeats can cause the same problems as terminal ones. Similarly, TTAGGG repeats induce chromosome rearrangements when introduced at an internal locus (Kilburn et al., 2001). The problems caused by chromosome-internal TTAGGG repeats also argue against the idea that the t loop structure plays a role in the replication defects.

Another possibility is that the telomeric DNA itself does not impair replication but becomes a challenge when bound to the telomeric protein complex. For instance, the single-stranded telomeric DNA binding protein POT1 may compete with RPA, thereby hampering lagging strand DNA synthesis. However, TTAGGG repeats also impair DNA replication in budding yeast (R. Wellinger, personal communication). Since budding yeast lacks shelterin, this result argues that TTAGGG repeats provide an inherent problem to the replication fork, regardless of the proteins bound or the presence of t loops.

We favor the view that the telomeric DNA is a problematic substrate for the replication machinery, most likely due to formation of G-G Hoogsteen base-paired G4 DNA in the G-rich telomeric repeat strand. Our finding that BLM and RTEL1, two helicases that have been implicated in the removal of G4 DNA, repress the fragile-telomere phenotype is consistent with the idea that the fork is primarily hindered by secondary structures formed by the G-rich telomeric DNA. If correct, this would predict that G4 ligands such as telomestatin and RHPS4 might induce a fragile-telomere phenotype and that some of their effects on the growth of tumor cells (Salvati et al., 2007; Tahara et al., 2006; Gomez et al., 2006) may be due to their preferential inhibition of telomere replication.

The Function of TRF1

Within shelterin, TRF2 and POT1 proteins collaborate to repress all DNA damage response pathways that threaten chromosome ends: DNA damage signaling by the ATM and ATR kinases and NHEJ- and HDR-mediated DSB repair. These functions are needed throughout the cell cycle, and loss of TRF2 or POT1 proteins in G0, G1, S, or G2 result in a DNA damage response (Celli and de Lange, 2005; Hockemeyer et al., 2006; Konishi and de Lange, 2008) (T.d.L., unpublished data). In contrast, TRF1 has a specific function in S phase, facilitating the replication of telomeres, thereby preventing ATR activation and the formation of fragile telomeres in metaphase.

Our data suggest that TRF1 primarily acts through the recruitment of BLM and RTEL1, but other factors are not excluded. Neither RTEL1 nor BLM were observed in an exhaustive PICh-based analysis of proteins associated with HeLa cell telomeres, although BLM was found at ALT telomeres (Dejardin and Kingston, 2009). However, it is possible that the association of these helicases is transient and therefore escapes detection.

Deletion of the presumed fission yeast ortholog of TRF1 and TRF2, Taz1, results in a block in telomere replication (Miller et al., 2006). When Taz1 is absent, 2D gels reveal an aberrant class telomeric fragments, referred to as the "plume," speculated to represent replication problems. Deletion of Taz1 also resulted in fork stalling at a chromosome-internal segment of telomeric DNA. Furthermore, the telomeres of *taz1*$^{-}$ cells are rapidly lost and require constant resynthesis by telomerase. These findings are consistent with a role for Taz1 in promoting replication through telomeric DNA and further underscore the similarity of fission yeast and mammalian telomeres (see also Miyoshi et al., 2008).

Implications

The finding that mammalian telomeres resemble fragile sites makes several predictions. Common fragile sites are prone to sister chromatid exchanges, often undergo rearrangements, and are frequent targets of integration of exogenous DNA (reviewed in Durkin and Glover, 2007). With regard to the first hallmark of common fragile sites, the fragile telomeres in TRF1 null cells do not appear to undergo frequent telomere sister chromatid exchanges (T-SCEs; Figure S2). However, T-SCEs are known to be repressed by TRF2 and POT1a/b, which remain associated with telomeres in TRF1 null cells (Celli et al., 2006; Palm et al., 2009).

With regard to the second hallmark of common fragile sites, their propensity to undergo rearrangements, recent work on focal deletions in colon carcinomas has been revealing. A large fraction (16%) of focal deletions occur near telomeres (Scott Powers, personal communication), consistent with genome rearrangements due to the fragile nature of telomeres and providing a parallel with the tumor-like microdeletions at common fragile sites (Arlt et al., 2009; Durkin et al., 2008). In addition, human chromosome ends show frequent duplications in subtelomeric sequences, and the rate of sister chromatid exchange is high near the telomeres (reviewed by Riethman, 2008). Both phenomena may be related to the fragile-telomere phenotype described here.

Finally, with regard to the integration of foreign DNA into common fragile sites, it is noteworthy that chromosome ends are often enriched for mobile elements. For instance, a human herpes virus (HHV-6) was recently show to preferentially integrate in telomeres (P.G. Medveczky, personal communication), and LINE-1 elements can transpose to telomeres in certain hamster cell lines (Morrish et al., 2007). An extreme version of telomere-tropic integration is found in the bdelloid rotifers, which have chromosome ends littered with foreign DNA, including mobile elements and DNA derived from horizontal gene transfer

A

TRF1$^{F/F}$	plasmid	Chromatid ends scored	Fragile Telomeres
- Cre		n= 2361	4%
+ Cre		n= 2068	17%
+ Cre	TRF1$^{\Delta Ac}$	n= 960	3%
+ Cre	TRF1$^{\Delta Myb}$	n= 1120	15%

C

Cells	Chromatid ends scored	Fragile Telomeres
Wildtype	n= 2384	4%
Blm$^{-/-}$	n= 4115	10%
Wrn$^{-/-}$	n= 1291	5%
Blm$^{-/-}$ *Wrn*$^{-/-}$	n= 4350	9%

B

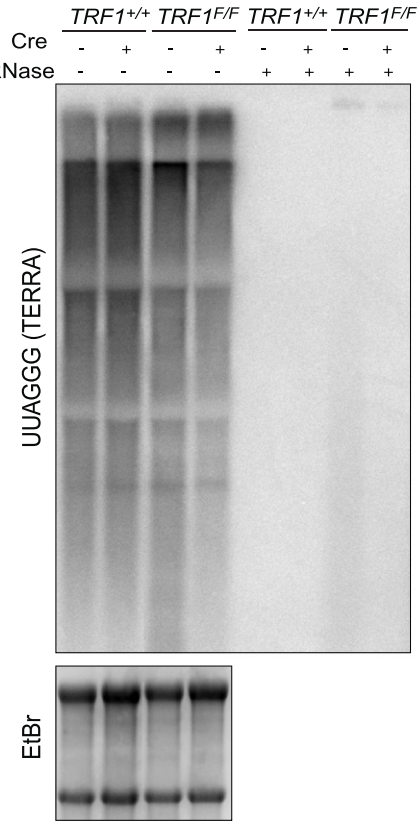

D

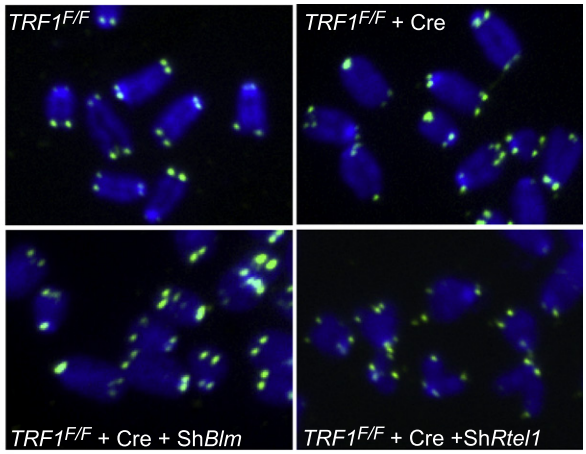

E

TRF1$^{F/F}$	ShRNA	Chromatid ends scored	Fragile Telomeres
- Cre		n= 1214, 1147	5%, 4%
+ Cre		n= 1134, 934	18%, 16%
- Cre	Sh*Blm*	n= 1044, 1068	9%, 8%
+ Cre	Sh*Blm*	n= 1780, 1430	14%, 14%
- Cre	Sh*Rtel1*	n= 1186, 1076	11%, 10%
+ Cre	Sh*Rtel1*	n= 2022, 1488	16%, 15%

F

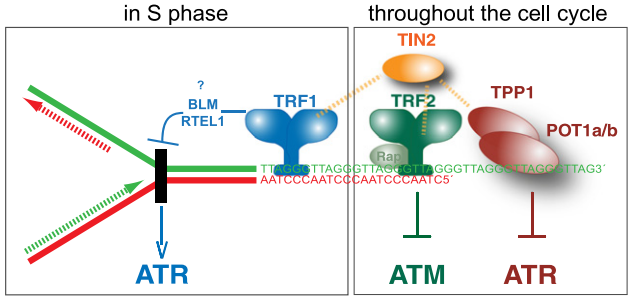

Figure 7. The Mechanism by which TRF1 Represses Telomere Fragility

(A) Frequency of fragile telomeres in Cre-treated *TRF1*$^{F/F}$ MEFs complemented with TRF1$^{\Delta Ac}$ or TRF1$^{\Delta Myb}$ (see Figure S6A for metaphase spreads and TRF1 immunoblots).

(B) TERRA detected by northern blotting of RNA from cells with the indicated genotype at day 4 after Cre. Bottom: Ethidium bromide (EtBr) staining of rRNAs serves as loading control.

(C) Fragile telomere incidence in cells lacking *Blm* and/or *Wrn*.

(D) Representative metaphase spreads from *TRF1*$^{F/F}$ MEFs (+ or − Cre treatment) infected with *Blm* and *Rtel1* shRNAs as indicated.

(E) Quantification of fragile telomeres in *TRF1*$^{F/F}$ MEFs (+ or − Cre treatment) infected with *Blm* and *Rtel1* shRNAs as indicated. See Figure S6 for validation of the shRNAs.

(Gladyshev et al., 2008). Although the preferred telomeric invasion in the bdelloid rotifers and mammalian cells could be due to addition of DNA to the termini of deprotected telomeres followed by telomere healing by telomerase, it is also possible that integration is biased by frequent replication fork arrest within the telomeric repeat array. In the latter scenario, the invading element is less likely to compromise telomere function. One could speculate that frequent fork arrest in subtelomeric/telomeric regions could have adaptive value since it would provide a safe sink for mobile elements that might otherwise invade more precious parts of the genome. This could explain why throughout eukaryotic evolution, telomeres have not evolved away from the TTAGGG repeats that generate replication problems.

EXPERIMENTAL PROCEDURES

TRF1 Gene Targeting, Isolation of MEFs, and Cell Culture Procedures

The mouse *TRF1* locus was modified using standard gene targeting techniques to generate the $TRF1^{F}$ and TRF^{-} genotypes shown in Figure 1. The targeting vector contained a TK-neomycin cassette flanked by LoxP sites cloned into a HindIII site in the first intron. A third LoxP site was introduced by insertion of an oligonucleotide into a PvuII site upstream of exon 1. ESC clones with the correct integration were identified by genomic blotting of HindIII-digested DNA with a probe flanking the left arm of the construct. Cre recombinase was transiently expressed in the clones to generate ES subclones that had lost the TK-neomycin cassette but retained exon 1 flanked by LoxP sites (floxed allele, F), and subclones that had lost both exon 1 and the TK-neomycin cassette (null allele, −). Two ESC subclones for each allele were used to generate chimeras that delivered offspring with the $TRF1^{F/+}$ or $TRF1^{+/-}$ genotypes. TRF1 mice were maintained in a mixed background (129/C57Bl6). Compound genotypes were created by intercrosses of $TRF1^{F/F}$ with $ATM^{+/-}$, $ATR^{F/-}$, $Lig4^{-/-}$, and *DNA-PKcs*$^{-/-}$ mice (Barlow et al., 1996; Brown and Baltimore, 2003; Gao et al., 1998). MEFs were isolated from E13.5 embryos and immortalized with pBabeSV40-LT (a gift from Greg Hannon). SV40-LT-immortalized $Wrn^{-/-}$, $Blm^{-/-}$, and $Wrn^{-/-}$ $Blm^{-/-}$ mouse ear fibroblasts were a gift from Brad Johnson. Cre recombinase was introduced with Hit&Run-Cre, Ad5 CMV Cre, or pWZL-Cre as described previously (Celli and de Lange, 2005). Aphidicolin treatments (0.2 μM) were for 16 hr. shRNAs for *Blm* (shBLM3c; GGACCTG CTGGAAGATTTA) and ATR (shATR3-1; Denchi and de Lange [2007]) were introduced using four infections at 6 hr intervals with pSuperior puromycin retrovirus. shRNA for *Rtel1* (pLK0.1 from Open Biosystems) was introduced using two lentiviral infections at 12 hr intervals.

Analysis of Telomeric DNA, IF, IF-FISH, Immunoblotting, FACS, and SA-β-Gal Assays

Telomeric overhang signals and telomeric restriction fragment patterns were determined by in-gel analysis as previously described (Celli and de Lange, 2005). FISH for telomeric DNA was performed with a C-strand PNA probe on methanol/acetic acid-fixed metaphase spreads as previously described (Dimitrova et al., 2008). For IF-FISH and immunoblotting, previously described standard methods were used (Celli and de Lange, 2005; Dimitrova et al., 2008). For FACS analysis, cells were plated at 1×10^6 cells and harvested 24 hr later. Ten micromolar BrdU was added to the media 1 hr prior to harvesting. Fixation was done with ice-cold 70% ethanol at 4°C for >30 min. Cells were washed twice with 0.5% BSA in PBS and resuspended in 0.4 ml 0.5% BSA in PBS containing 5 μg propidium-iodide and RNaseA (100 μg/ml). Samples were analyzed with a FACScalibur flow cytometer (Becton Dickinson) with FlowJo software. SA-β-GAL staining was preformed for 8–16 hr at 37°C as previously described (Dimri et al., 1995).

SMARD Assay

The SMARD assay was performed essentially as described previously (Norio and Schildkraut, 2001). Cells were sequentially labeled with 25 μM IdU (30 min or 1 hr) and 25 μM CldU (30 min or 1 hr) with three PBS washes in between followed by incubation with media without IdU/CldU for 3 hr. This process was repeated six times for 30 min pulses and three times for 1 hr pulses. DNA isolation and processing for SMARD were as described previously (Norio and Schildkraut, 2001). DNA was stretched on microscope slides coated with 3-aminopropyltriethoxysilane (Sigma). After stretching, the DNA was denatured in alkali-denaturing buffer (0.1 N NaOH in 70% ethanol and 0.1% b-mercaptothanoland) for 8, 12, or 15 min and fixed by addition of 0.5% glutaraldehyde for 5 min. Telomeric DNA was identified by hybridization with a Biotin-OO-(CCCTAA)4 PNA probe and Alexa Fluor 350-conjugated NeutrAvidin antibody (Molecular Probes) followed by biotinylated anti-avidin antibody (Vector). Halogenated nucleotides were detected with a mouse anti-IdU monoclonal antibody (Becton Dickinson) and a rat anti-CldU monoclonal antibody (Accurate). Alexa Fluor 568-conjugated goat anti-mouse (Molecular Probes) and Alexa Fluor 488-conjugated goat anti-rat were used as secondary antibodies (Molecular Probes).

Telomeric ChIP Analysis

IP of telomeric chromatin was performed as previously described (Loayza and de Lange, 2003) and analyzed by dot-blotting using a TTAGGG repeat probe and a BamHI repeat probe as a negative control. Input DNA was used to calculate the % telomeric DNA brought down in the ChIPs. The following antibodies were used as crude sera: TRF1, 1449 (rabbit polyclonal); TRF2, 1254 (rabbit polyclonal); Rap1, 1252 (rabbit polyclonal); POT1a, 1220 (rabbit polyclonal); and TPP1, 1150 (rabbit polyclonal).

TERRA Analysis

Total cellular RNA was prepared with the RNeasy Mini Kit (QIAGEN), according to the manufacturer's instructions, and northern blot analysis was performed as previously described (Azzalin et al., 2007). Blots were prehybridized at 60°C for 1 hr in Church mix (0.5 M Na_2HPO_4 [pH 7.2], 1 mM EDTA, 7% SDS, and 1% BSA), followed by hybridization at 60°C overnight with 800 bp telomeric DNA probe from pSP73Sty11 labeled with a C-strand primer, Klenow polymerase, and α-[^{32}P]-dCTP. The blot was exposed to a PhosphorImager screen and scanned with Image-Quant software.

SUPPLEMENTAL DATA

Supplemental Data include Supplemental Experimental Procedures and seven figures and can be found with this article online at http://www.cell.com/supplemental/S0092-8674(09)00721-1.

ACKNOWLEDGMENTS

We thank Devon White for expert mouse husbandry and Eros Lazzerini Denchi for assistance with protocols and helpful discussion. Megan van Overbeek is thanked for assistance with TRF1 antibody, and members of the de Lange laboratory are thanked for comments on these experiments. We are grateful to Sara Buonomo for the BLM shRNA and to Brad Johnson for providing the $Blm^{-/-}$, $Wrn^{-/-}$, and $Blm^{-/-}$ $Wrn^{-/-}$ cell lines. We thank Scott Powers, Peter Medveczky, and Raymund Wellinger for allowing us to cite unpublished data. A.S. is supported by a postdoctoral fellowship from Susan G. Komen for the Cure. This work was supported by grants from the National Institutes of Health to T.d.L. and C.L.S. The targeting construct and the conditional TRF1 knockout strain were generated by J.K. and D.H. A.S. generated compound genotypes, isolated MEFs, and performed all other experiments with the exception of the human telomere length study (S.L.M.). All SMARD analysis was performed by A.S. with the help of S.T.K. and C.L.S. T.d.L. and A.S. designed the experiments, wrote the paper, and made the figures.

(F) Schematic summarizing the proposed function of TRF1 in the context of shelterin. While TRF2 and POT1 repress the DNA damage response throughout the cell cycle, TRF1 is proposed to act in S phase to facilitate replication fork progression through the telomeric DNA. TRF1 is proposed to prevent formation of a fork barrier (most likely G4 DNA) in part by acting with BLM and RTEL1.

Received: February 25, 2009
Revised: May 19, 2009
Accepted: June 11, 2009
Published: July 9, 2009

REFERENCES

Adams, A.K., and Holm, C. (1996). Specific DNA replication mutations affect telomere length in Saccharomyces cerevisiae. Mol. Cell. Biol. *16*, 4614–4620.

Anglana, M., Apiou, F., Bensimon, A., and Debatisse, M. (2003). Dynamics of DNA replication in mammalian somatic cells: nucleotide pool modulates origin choice and interorigin spacing. Cell *114*, 385–394.

Arlt, M.F., Xu, B., Durkin, S.G., Casper, A.M., Kastan, M.B., and Glover, T.W. (2004). BRCA1 is required for common-fragile-site stability via its G2/M checkpoint function. Mol. Cell. Biol. *24*, 6701–6709.

Arlt, M.F., Mulle, J.G., Schaibley, V.M., Ragland, R.L., Durkin, S.G., Warren, S.T., and Glover, T.W. (2009). Replication stress induces genome-wide copy number changes in human cells that resemble polymorphic and pathogenic variants. Am. J. Hum. Genet. *84*, 339–350.

Atanasiu, C., Deng, Z., Wiedmer, A., Norseen, J., and Lieberman, P.M. (2006). ORC binding to TRF2 stimulates OriP replication. EMBO Rep. *7*, 716–721.

Azzalin, C.M., Reichenbach, P., Khoriauli, L., Giulotto, E., and Lingner, J. (2007). Telomeric repeat containing RNA and RNA surveillance factors at mammalian chromosome ends. Science *318*, 798–801.

Barber, L.J., Youds, J.L., Ward, J.D., McIlwraith, M.J., O'Neil, N.J., Petalcorin, M.I., Martin, J.S., Collis, S.J., Cantor, S.B., Auclair, M., et al. (2008). RTEL1 maintains genomic stability by suppressing homologous recombination. Cell *135*, 261–271.

Barlow, C., Hirotsune, S., Paylor, R., Liyanage, M., Eckhaus, M., Collins, F., Shiloh, Y., Crawley, J.N., Ried, T., Tagle, D., and Wynshaw-Boris, A. (1996). Atm-deficient mice: a paradigm of ataxia telangiectasia. Cell *86*, 159–171.

Becker, N.A., Thorland, E.C., Denison, S.R., Phillips, L.A., and Smith, D.I. (2002). Evidence that instability within the FRA3B region extends four megabases. Oncogene *21*, 8713–8722.

Blanco, R., Munoz, P., Flores, J.M., Klatt, P., and Blasco, M.A. (2007). Telomerase abrogation dramatically accelerates TRF2-induced epithelial carcinogenesis. Genes Dev. *21*, 206–220.

Brown, E.J., and Baltimore, D. (2003). Essential and dispensable roles of ATR in cell cycle arrest and genome maintenance. Genes Dev. *17*, 615–628.

Carson, M.J., and Hartwell, L. (1985). CDC17: an essential gene that prevents telomere elongation in yeast. Cell *42*, 249–257.

Casper, A.M., Nghiem, P., Arlt, M.F., and Glover, T.W. (2002). ATR regulates fragile site stability. Cell *111*, 779–789.

Celli, G.B., and de Lange, T. (2005). DNA processing not required for ATM-mediated telomere damage response after TRF2 deletion. Nat. Cell Biol. *7*, 712–718.

Celli, G.B., Lazzerini Denchi, E., and de Lange, T. (2006). Ku70 stimulates fusion of dysfunctional telomeres yet protects chromosome ends from homologous recombination. Nat. Cell Biol. *8*, 885–890.

Chan, K.L., Palmai-Pallag, T., Ying, S., and Hickson, I.D. (2009). Replication stress induces sister-chromatid bridging at fragile site loci in mitosis. Nat. Cell Biol. *11*, 753–760.

Chen, Y., Yang, Y., van Overbeek, M., Donigian, J.R., Baciu, P., de Lange, T., and Lei, M. (2008). A shared docking motif in TRF1 and TRF2 used for differential recruitment of telomeric proteins. Science *319*, 1092–1096.

Chong, L., van Steensel, B., Broccoli, D., Erdjument-Bromage, H., Hanish, J., Tempst, P., and de Lange, T. (1995). A human telomeric protein. Science *270*, 1663–1667.

de Lange, T. (2005). Shelterin: the protein complex that shapes and safeguards human telomeres. Genes Dev. *19*, 2100–2110.

Dejardin, J., and Kingston, R.E. (2009). Purification of proteins associated with specific genomic Loci. Cell *136*, 175–186.

Denchi, E.L., and de Lange, T. (2007). Protection of telomeres through independent control of ATM and ATR by TRF2 and POT1. Nature *448*, 1068–1071.

Deng, Z., Dheekollu, J., Broccoli, D., Dutta, A., and Lieberman, P.M. (2007). The origin recognition complex localizes to telomere repeats and prevents telomere-circle formation. Curr. Biol. *17*, 1989–1995.

Dimitrova, N., Chen, Y.C., Spector, D.L., and de Lange, T. (2008). 53BP1 promotes non-homologous end joining of telomeres by increasing chromatin mobility. Nature *456*, 524–528.

Dimri, G.P., Lee, X., Basile, G., Acosta, M., Scott, G., Roskelley, C., Medrano, E.E., Linskens, M., Rubelj, I., Pereira-Smith, O., et al. (1995). A biomarker that identifies senescent human cells in culture and in aging skin in vivo. Proc. Natl. Acad. Sci. USA *92*, 9363–9367.

Ding, H., Schertzer, M., Wu, X., Gertsenstein, M., Selig, S., Kammori, M., Pourvali, R., Poon, S., Vulto, I., Chavez, E., et al. (2004). Regulation of murine telomere length by Rtel: an essential gene encoding a helicase-like protein. Cell *117*, 873–886.

Durkin, S.G., and Glover, T.W. (2007). Chromosome fragile sites. Annu. Rev. Genet. *41*, 169–192.

Durkin, S.G., Ragland, R.L., Arlt, M.F., Mulle, J.G., Warren, S.T., and Glover, T.W. (2008). Replication stress induces tumor-like microdeletions in FHIT/FRA3B. Proc. Natl. Acad. Sci. USA *105*, 246–251.

Fairall, L., Chapman, L., Moss, H., de Lange, T., and Rhodes, D. (2001). Structure of the TRFH dimerization domain of the human telomeric proteins TRF1 and TRF2. Mol. Cell *8*, 351–361.

Falaschi, A., Abdurashidova, G., Sandoval, O., Radulescu, S., Biamonti, G., and Riva, S. (2007). Molecular and structural transactions at human DNA replication origins. Cell Cycle *6*, 1705–1712.

Feichtinger, W., and Schmid, M. (1989). Increased frequencies of sister chromatid exchanges at common fragile sites (1)(q42) and (19)(q13). Hum. Genet. *83*, 145–147.

Gao, Y., Chaudhuri, J., Zhu, C., Davidson, L., Weaver, D.T., and Alt, F.W. (1998). A targeted DNA-PKcs-null mutation reveals DNA-PK-independent functions for KU in V(D)J recombination. Immunity *9*, 367–376.

Gladyshev, E.A., Meselson, M., and Arkhipova, I.R. (2008). Massive horizontal gene transfer in bdelloid rotifers. Science *320*, 1210–1213.

Glover, T.W., Berger, C., Coyle, J., and Echo, B. (1984). DNA polymerase alpha inhibition by aphidicolin induces gaps and breaks at common fragile sites in human chromosomes. Hum. Genet. *67*, 136–142.

Glover, T.W., and Stein, C.K. (1987). Induction of sister chromatid exchanges at common fragile sites. Am. J. Hum. Genet. *41*, 882–890.

Gomez, D., Wenner, T., Brassart, B., Douarre, C., O'Donohue, M.F., El Khoury, V., Shin-Ya, K., Morjani, H., Trentesaux, C., and Riou, J.F. (2006). Telomestatin-induced telomere uncapping is modulated by POT1 through G-overhang extension in HT1080 human tumor cells. J. Biol. Chem. *281*, 38721–38729.

Greider, C.W., and Blackburn, E.H. (1985). Identification of a specific telomere terminal transferase activity in Tetrahymena extracts. Cell *43*, 405–413.

Hockemeyer, D., Daniels, J.P., Takai, H., and de Lange, T. (2006). Recent expansion of the telomeric complex in rodents: Two distinct POT1 proteins protect mouse telomeres. Cell *126*, 63–77.

Huber, M.D., Lee, D.C., and Maizels, N. (2002). G4 DNA unwinding by BLM and Sgs1p: substrate specificity and substrate-specific inhibition. Nucleic Acids Res. *30*, 3954–3961.

Huber, M.D., Duquette, M.L., Shiels, J.C., and Maizels, N. (2006). A conserved G4 DNA binding domain in RecQ family helicases. J. Mol. Biol. *358*, 1071–1080.

Iwano, T., Tachibana, M., Reth, M., and Shinkai, Y. (2004). Importance of TRF1 for functional telomere structure. J. Biol. Chem. *279*, 1442–1448.

Karlseder, J., Kachatrian, L., Takai, H., Mercer, K., Hingorani, S., Jacks, T., and de Lange, T. (2003). Targeted deletion reveals an essential function for the telomere length regulator Trf1. Mol. Cell. Biol. *23*, 6533–6541.

Kilburn, A.E., Shea, M.J., Sargent, R.G., and Wilson, J.H. (2001). Insertion of a telomere repeat sequence into a mammalian gene causes chromosome instability. Mol. Cell. Biol. *21*, 126–135.

Konishi, A., and de Lange, T. (2008). Cell cycle control of telomere protection and NHEJ revealed by a ts mutation in the DNA-binding domain of TRF2. Genes Dev. *22*, 1221–1230.

LeBeau, M.M., and Rowley, J.D. (1984). Heritable fragile sites in cancer. Nature *308*, 607–608.

Lillard-Wetherell, K., Machwe, A., Langland, G.T., Combs, K.A., Behbehani, G.K., Schonberg, S.A., German, J., Turchi, J.J., Orren, D.K., and Groden, J. (2004). Association and regulation of the BLM helicase by the telomere proteins TRF1 and TRF2. Hum. Mol. Genet. *13*, 1919–1932.

Loayza, D., and de Lange, T. (2003). POT1 as a terminal transducer of TRF1 telomere length control. Nature *424*, 1013–1018.

Luo, G., Santoro, I.M., McDaniel, L.D., Nishijima, I., Mills, M., Youssoufian, H., Vogel, H., Schultz, R.A., and Bradley, A. (2000). Cancer predisposition caused by elevated mitotic recombination in Bloom mice. Nat. Genet. *26*, 424–429.

Miller, K.M., Rog, O., and Cooper, J.P. (2006). Semi-conservative DNA replication through telomeres requires Taz1. Nature *440*, 824–828.

Miyoshi, T., Kanoh, J., Saito, M., and Ishikawa, F. (2008). Fission yeast Pot1-Tpp1 protects telomeres and regulates telomere length. Science *320*, 1341–1344.

Morrish, T.A., Garcia-Perez, J.L., Stamato, T.D., Taccioli, G.E., Sekiguchi, J., and Moran, J.V. (2007). Endonuclease-independent LINE-1 retrotransposition at mammalian telomeres. Nature *446*, 208–212.

Musio, A., Rainaldi, G., and Sbrana, I. (1996). Spontaneous and aphidicolin-sensitive fragile site 3cen co-localizes with the (TTAGGG)n telomeric sequence in Chinese hamster cells. Cytogenet. Cell Genet. *75*, 159–163.

Norio, P., and Schildkraut, C.L. (2001). Visualization of DNA replication on individual Epstein-Barr virus episomes. Science *294*, 2361–2364.

Norio, P., Kosiyatrakul, S., Yang, Q., Guan, Z., Brown, N.M., Thomas, S., Riblet, R., and Schildkraut, C.L. (2005). Progressive activation of DNA replication initiation in large domains of the immunoglobulin heavy chain locus during B cell development. Mol. Cell *20*, 575–587.

Okamoto, K., Iwano, T., Tachibana, M., and Shinkai, Y. (2008). Distinct roles of TRF1 in the regulation of telomere structure and lengthening. J. Biol. Chem. *283*, 23981–23988.

Palm, W., and de Lange, T. (2008). How shelterin protects mammalian telomeres. Annu. Rev. Genet. *42*, 301–334.

Palm, W., Hockemeyer, D., Kibe, T., and de Lange, T. (2009). Functional dissection of human and mouse POT1 proteins. Mol. Cell. Biol. *29*, 471–482.

Philippe, C., Coullin, P., and Bernheim, A. (1999). Double telomeric signals on single chromatids revealed by FISH and PRINS. Ann. Genet. *42*, 202–209.

Riethman, H. (2008). Human telomere structure and biology. Annu. Rev. Genomics Hum. Genet. *9*, 1–19.

Salvati, E., Leonetti, C., Rizzo, A., Scarsella, M., Mottolese, M., Galati, R., Sperduti, I., Stevens, M.F., D'Incalci, M., Blasco, M., et al. (2007). Telomere damage induced by the G-quadruplex ligand RHPS4 has an antitumor effect. J. Clin. Invest. *117*, 3236–3247.

Schoeftner, S., and Blasco, M.A. (2008). Developmentally regulated transcription of mammalian telomeres by DNA-dependent RNA polymerase II. Nat. Cell Biol. *10*, 228–236.

Smogorzewska, A., van Steensel, B., Bianchi, A., Oelmann, S., Schaefer, M.R., Schnapp, G., and de Lange, T. (2000). Control of human telomere length by TRF1 and TRF2. Mol. Cell. Biol. *20*, 1659–1668.

Sun, H., Karow, J.K., Hickson, I.D., and Maizels, N. (1998). The Bloom's syndrome helicase unwinds G4 DNA. J. Biol. Chem. *273*, 27587–27592.

Tahara, H., Shin-Ya, K., Seimiya, H., Yamada, H., Tsuruo, T., and Ide, T. (2006). G-Quadruplex stabilization by telomestatin induces TRF2 protein dissociation from telomeres and anaphase bridge formation accompanied by loss of the 3′ telomeric overhang in cancer cells. Oncogene *25*, 1955–1966.

Takai, H., Smogorzewska, A., and de Lange, T. (2003). DNA damage foci at dysfunctional telomeres. Curr. Biol. *13*, 1549–1556.

Tatsumi, Y., Ezura, K., Yoshida, K., Yugawa, T., Narisawa-Saito, M., Kiyono, T., Ohta, S., Obuse, C., and Fujita, M. (2008). Involvement of human ORC and TRF2 in pre-replication complex assembly at telomeres. Genes Cells *13*, 1045–1059.

Ten Hagen, K.G., Gilbert, D.M., Willard, H.F., and Cohen, S.N. (1990). Replication timing of DNA sequences associated with human centromeres and telomeres. Mol. Cell. Biol. *10*, 6348–6355.

Undarmaa, B., Kodama, S., Suzuki, K., Niwa, O., and Watanabe, M. (2004). X-ray-induced telomeric instability in Atm-deficient mouse cells. Biochem. Biophys. Res. Commun. *315*, 51–58.

van Overbeek, M., and de Lange, T. (2006). Apollo, an Artemis-related nuclease, interacts with TRF2 and protects human telomeres in S phase. Curr. Biol. *16*, 1295–1302.

van Steensel, B., and de Lange, T. (1997). Control of telomere length by the human telomeric protein TRF1. Nature *385*, 740–743.

Wright, W.E., Tesmer, V.M., Liao, M.L., and Shay, J.W. (1999). Normal human telomeres are not late replicating. Exp. Cell Res. *251*, 492–499.

Yunis, J.J., and Soreng, A.L. (1984). Constitutive fragile sites and cancer. Science *226*, 1199–1204.

Supplemental Data

Mammalian Telomeres Resemble

Fragile Sites and Require TRF1

for Efficient Replication

Agnel Sfeir, Settapong T. Kosiyatrakul, Dirk Hockemeyer, Sheila L. MacRae, Jan Karlseder, Carl L. Schildkraut, and Titia de Lange

Supplemental Experimental Procedures

Cell culture and retroviral infection

MEFs were isolated from E13.5 embryos and cultured in DMEM supplemented with 1 mM Na-pyruvate, 100 U of penicillin per ml, 0.1 μg of streptomycin per ml, 0.2 mM L-glutamine, 0.1 mM nonessential amino acids, and 15% (vol/vol) fetal calf serum (FCS). Immortalized MEFs were cultured in media with 10% FCS without sodium pyruvate. Cre recombinase was introduced using Hit&Run-Cre (Silver and Livingston, 2001), Ad5 CMV Cre (Resource Center, The University of Iowa, Iowa City, IA), or pWZL-Cre as described previously (Celli and de Lange, 2005). Treatments of cultured cells were as follows: Synchronization of cells in G_0 was performed with primary MEF lines by contact inhibition and serum starvation. Primary MEFs were plated at $1*10^6$ cells per 10 cm dish or $0.5*10^6$ cells per 6 cm dish in media supplemented with 15% FCS. When cells reached confluence, serum levels were dropped gradually to 0.5% over a period of 5 days and the cells were maintained for an additional 2 days in media with 0.5% serum. Subsequently, cells were infected twice with Ad5-CMV-Cre (m.o.i. of 1000) and harvested 4 days later. shRNAs for Blm and ATR were introduced using 4 infections at 6 hr intervals of the shRNA bearing pSuperior puromycin retrovirus-containing supernatants from Phoenix cells supplemented with 4 μg/ml polybrene. Parallel infection with shLuciferase was used as a negative control. shRNA for Rtel1 was introduced using 2 infections at 12 hr intervals of lentivirus-containing supernatant from 293T cells. Parallel infection with PLK0.1 was used as a negative control. Puromycin selection was applied for 3 days at 2 μg/ml. Full-length mouse TRF1 (aa 2-421), $TRF1^{\Delta Ac}$ (aa 55-421) and $TRF1^{\Delta Myb}$ (aa 2-363) were cloned into pLPC-puro retroviral expression vector and introduced into MEFs by 3 retroviral infections at 12 hour intervals using supernatant from transfected Phoenix cells. Puromycin selection was applied for 3 days at 2 μg/ml.
SV40 Large T immortalized $Wrn^{-/-}$, $Blm^{-/-}$, and $Wrn^{-/-}$ $Blm^{-/-}$ mouse ear fibroblasts (a gift from Brad Johnson) were cultured in DMEM media containing 10% fetal calf serum (FCS). The BLM mutation is a hypomorphic allele BLM^{m3} that has been previously shown to induce high levels of homologous recombination and increased rates of loss of heterozygosity (Luo et al., 2000). HeLa 1.3, BJ-hTERT and HTC75 cells were cultured in DMEM media supplemented with 10% bovine calf serum (BCS).

TRF1 gene targeting

The mTRF1 locus was isolated from 129 SV BAC library (Genome Systems) using full-length cDNA as a probe. The targeting vector contained a TK-Neomycin cassette flanked by Lox P sites cloned into a HindIII site in the first intron. A third Lox P site was

introduced by inserting an oligonucleotide into a PvuII site upstream of exon 1. ES clones with the correct integration were identified by genomic blotting of HindIII digested DNA using a probe flanking the left arm of the construct. Cre recombinase was transiently expressed in the targeted ES clones to generate ES subclones that had lost the TK-neomycin cassette but retained exon 1 flanked by LoxP sites (floxed allele, F) and subclones that had lost both exon 1 and the TK-neomycin cassette (null allele, -). Two ES cell subclones for each allele were used to generate chimeras, which delivered offspring with the $TRF1^{F/+}$ or $TRF1^{+/-}$ genotypes. TRF1 mice were maintained in a mixed background (129/C57Bl6). Genotyping PCR for TRF1 was performed using the following primers: F2: TGCTGCTGCTGCCATAACGCTCAA; F1: TATACTTACAGCGCTGGGAAG; and R: GGCCAAAAGACGGAAATTTGA. The amplification reaction was performed in a volume of 25 μl containing 1 μl DNA, 25 pmol of each primer, 0.1 μM dNTPs, 1.5 mM MgCl2, 50 mM KCl, 10 mM Tris-HCl (pH 8.0), and 0.5 U of Taq polymerase (Takara Taq). PCR conditions were as follows: 95°C for 1 min, 35 rounds of 95°C for 30 sec, 57°C for 45 sec, and 72°C for 1 min and 72°C for 5 min.

Analysis of telomeric DNA by pulse-field gel electrophoresis and in-gel hybridization

Telomeric overhang signals and telomeric restriction fragment patterns were determined by in-gel analysis as previously described (Celli and de Lange, 2005). Briefly, a [CCCTAA]4 oligonucleotide was hybridized to native MboI cut genomic DNA fractionated on CHEF gels to determine the overhang signal. The DNA was denatured in situ, neutralized, and then rehybridized with the same probe to determine the total telomeric DNA signals. The overhang signal in each lane is normalized to the duplex telomeric signal so that comparison of these ratios reveal changes in the overhang status.

Telomere FISH and CO-FISH on metaphase spreads

FISH for telomeric DNA was performed as previously described (Dimitrova et al., 2008). Briefly, cells at the indicated time points and treatments were incubated for 1.5 h with 0.2 μg/ml colcemid. The cells were harvested, swollen in KCl, fixed in methanol/acetic acid (3:1) and dropped onto glass slides in a Thermotron Cycler (20^0C, 50% humidity). After aging overnight, the slides were washed in 1X PBS for 5 minutes followed by consecutive incubation with 75%, 95% and 100% ethanol. The slides were allowed to air dry for 30 minutes before applying Hybridizing Solution (70% formamide, 1 mg/ml blocking reagent (Roche), 10 mM Tris-HCl pH 7.2) containing FITC-OO-(CCCTAA)3 PNA probe (Applied Biosystems). The spreads were denatured for 3 min at 80ºC on a heat block and hybridized at RT for 2 hours. The slides were washed twice with 70% formamide/10 mM Tris-HCl (15 minutes each wash), followed by three washes in 0.1 M Tris-HCl, pH 7.0/0.15 M NaCl/0.08% Tween-20 (5 minutes each). The chromosomal DNA was counterstained with 4,6-diamidino-2-phenylindole (DAPI) added to the second wash. Slides were mounted in antifade reagent (ProLong Gold, Invitrogen) and digital images were captured with a Zeiss Axioplan II microscope with a Hamamatsu C4742-95 camera using Improvision OpenLab software.

For CO-FISH the cells were treated with 10 μM BrdU:BrdC (3:1) for 16 h and colcemid was added for the last 1.5 hour at a concentration of 0.2 μg/ml. Prior to hybridization the slides were treated with RNase A (0.5 μg/ml in PBS) for 10 min at 37^0C, stained with Hoechst 33258 (0.5 μg/ml in 2XSSC) for 10 min at RT and exposed to 365-nm UV light (Stratalinker 1800 UV irradiator) for 30 min. The BrdU/dC substituted DNA strand was digested with Exonuclease III (10 U/ml) for 10 min at RT. The slides were dehydrated

through an ethanol series (75%, 95% and 100%) as above and hybridized with TAMRA-OO-(TTAGGG)3 PNA probe in hybridization solution for 2 hours. The slides were washed for few seconds with 70% formamide/10 mM Tris-HCl pH 7.2 and incubated with FITC-OO-(CCCTAA)3 PNA probe in hybridization solution for 2 hours. The subsequent steps were as for the FISH protocol.

Immunoblotting

Cells were harvested by trypsinization, suspended in media with serum, washed with PBS and lysed in Laemmli buffer (100 mM Tris-HCl pH 6.8, 200 mM DTT, 3% SDS, 20% glycerol, 0.05% bromophenol blue) at $1*10^4$ cell per µl. The lysate was denatured for 10 min at 95^0C, and sheared (10 times) by forcing it through an insulin needle. Per lane, lysate from 10^5 cells was resolved on SDS/PAGE (5% for ATM and ATR and 10% for all other proteins), transferred to a membrane, and blocked in PBS with 5% milk/0.1%Tween-20. The following primary antibodies were incubated in PBS/5% milk/0.1% Tween-20: TRF1 (1449, rabbit polyclonal); TRF2 (1254, rabbit polyclonal); Rap1 (1252, rabbit polyclonal); POT1a (1220, rabbit polyclonal); Chk2 (mouse monoclonal, BD Biosciences); Phopho-Chk1 (Ser 345) (mouse monoclonal, Cell Signaling); Chk1 (mouse monoclonal, Santa Cruz); ATM (mouse monoclonal, MAT3, Sigma); ATR (N-19) (goat polyclonal, Santa Cruz); BLM (rabbit polyclonal, Bethyl Laboratories); α-tubulin (clone GTU 88, Sigma). After incubation with the appropriate secondary antibody, immunoblots were developed with enhanced chemiluminescence (ECL, Amersham).

IF-FISH and TIF assay

All steps were performed at room temperature unless indicated otherwise. Cells grown on coverslips were fixed for 10 min in 2% paraformaldehyde followed by three 5-min washes with PBS. For indirect immunofluorescence, coverslips were incubated in Blocking Solution (1 mg/ml BSA, 3% goat serum, 0.1% Triton X-100, 1 mM EDTA in PBS) for 30 min, followed by incubation with primary antibodies in Blocking Solution for 2 hours: 53BP1, 100-304A (rabbit polyclonal, Novus Biologicals); TRF1, 1449 (affinity purified rabbit polyclonal, raised against a GST-fusion of mouse TRF1 without the Myb domain); α-H2AX, mouse monoclonal (Upstate Biotechnology); Rap1, 1252 (affinity purified rabbit polyclonal). After three 5-min washes with PBS, the coverslips were incubated with Rhodamine Red-X labeled secondary antibody raised against rabbit (RRX, Jackson) for 30 min and washed 3 times in PBS. Coverslips were dehydrated in 70%, 95% and 100% ethanol, 5 min each, and allowed to air dry. FITC-OO-(CCCTAA)3 (Applied Biosystems) PNA probe in Blocking Solution (70% formamide, 1 mg/ml blocking reagent (Roche), 10 mM Tris-HCl pH 7.2) was added and the coverslips were denatured on a heat block (10 min at 80ºC). Hybridization was for 4 hours in the dark. The coverslips were washed twice with 70% formamide, 10 mM Tris-HCl pH 7.2 for 15 min and three times in PBS. DNA was counterstained with DAPI and slides were mounted in antifade reagent (ProLong Gold, Invitrogen). Digital images were captured with a Zeiss Axioplan II microscope with a Hamamatsu C4742-95 camera using Improvision OpenLab software. For the TIF assay, cells with at least five telomeric 53BP1 foci were scored as TIF positive; n>100 for each experiment. Data reported are averages of three independent experiments and error bars indicate the standard deviations.

FACS

One day before harvesting, $1*10^6$ cells were plated on 10 cm dishes. 10 µM BrdU was added one hour prior harvesting. Cells were collected by trypsinization, washed in PBS, and resuspended in PBS with 1 mM EDTA. Cells were fixed with ice cold 70% ethanol at

40^0C for at least 30 min. Cells were washed twice with 0.5% BSA in PBS and re-suspended in 0.4 ml 0.5% BSA in PBS containing 5 μg propidium-iodide and RNAseA (100 μg/ml). Samples were analyzed with a FACS calibur flow cytometer (Becton Dickinson) using FlowJo software.

Senescence-associated β-galactosidase staining

SA-β-GAL staining was preformed as previously described (Dimri et al., 1995). $TRF1^{F/F}$ cells were infected with vector control or pWZL Cre and selected with hygromycin for 5 days. At day 6 after infection $1*10^5$ cells were plated in a 6-well cell culture plate. The following day, the cells were fixed with 2% formaldehyde and 0.2% glutaraldehyde in PBS for 3 minutes and washed twice in PBS. The cells were then incubated with 3 ml of SA-β-GAL stain (1 mg/ml 5-bromo-4-chloro-3-indolyl β-D-galactoside (X-Gal), 40 mM citric acid/sodium phosphate, pH 6.0, 5 mM potassium ferrocyanide, 5 mM potassium ferricyanide, 150 mM NaCl, 2 mM $MgCl_2$) at 37°C for 8 to 16 hrs in the dark. Cells were washed twice with PBS and photographed.

ChIP analysis

ChIP was performed as previously described (Loayza and de Lange, 2003). The TTAGGG signal was normalized to BamHI repeats. The following antibodies were used as crude sera: TRF1, 1449 (rabbit polyclonal); TRF2, 1254 (rabbit polyclonal); Rap1, 1252 (rabbit polyclonal); POT1a, 1220 (rabbit polyclonal); TPP1, 1150 (rabbit polyclonal).

Northern for TERRA

Total cellular RNA was prepared using RNeasy Mini Kit (Qiagen), according to the manufacturer instructions and Northern blot analysis was performed as previously described (Azzalin et al., 2007). Briefly, 10 μg RNA was loaded onto 1.3% formaldehyde agarose gels and separated by gel electrophoresis. RNA was transferred to a Hybond membrane. The blot was prehybridized at 60°C for 1 h in Church mix (0.5 M Na_2HPO_4 (pH 7.2), 1 mM EDTA, 7% SDS, and 1% BSA), followed by hybridization at 60°C overnight with 800-bp telomeric DNA probe from pSP73Sty11 labeled by Klenow fragment and [32P]dCTP. The blot was exposed to a PhosphorImager screen and scanned using Image-Quant software.

Telomere Length analysis

Cells were harvested by trypsinization, washed with cold Phosphate Buffered Saline (PBS), and lysed in Tris/NaCl/EDTA/SDS (TNE,10 mM Tris-HCl pH 7.4, 100 mM NaCl, 10 mM EDTA, 0.1%SDS) containing 0.1 mg/ml proteinase K at 37°C o/n. Two phenol extraction steps with phenol/chloroform/isoamyl-alcohol (50:49:1) were performed in phase-lock tubes (Eppendorf). DNA was precipitated with iso-propanol and NaOAc, dissolved in TE (10 mM Tris-HCl pH 7.4, 1 mM EDTA) and digested with MboI/AluI. DNA concentrations were measured by Hoechst fluorimetry and 2 μg of DNA was fractionated on a 0.7% agarose gel. Hybridizations, washes and signal detection were performed as described by (Smogorzewska et al., 2000).

Semi quantitative RT-PCR analysis

Total cellular RNA was prepared from MEFs using RNeasy Mini Kit (Qiagen). 1 μg of RNA was subjected to reverse transcription using random oligo primer and ThermoScript RT-PCR System (Invitrogen) according to the manufacturer's protocol. Mouse RTEL1 cDNA was amplified by PCR with sense: 5'- CCT GAA TGG TGT GAC AGT GG-3' and

antisense: 5'- CAG GAT GAC AAG GTC CGA CT- 3'; GAPDH cDNA was amplified by PCR with sense: 5'- GGG TGA GGC CGG TGC TGA GTA T -3' and antisense 5'- TTG GGG GTA GGA ACA CGG AAG G -3'. The PCR reaction consisted of denaturing for 30 sec at 94^0C, annealing for 40 sec at 58^0C and elongation for 30 sec at 72^0C. The PCR products were examined at the indicated number of the cycles.

Supplemental References

Azzalin, C. M., Reichenbach, P., Khoriauli, L., Giulotto, E., and Lingner, J. (2007). Telomeric repeat containing RNA and RNA surveillance factors at mammalian chromosome ends. Science *318*, 798-801.

Celli, G., and de Lange, T. (2005). DNA processing not required for ATM-mediated telomere damage response after TRF2 deletion. Nat Cell Biol *7*, 712-718.

Dimitrova, N., Chen, Y. C., Spector, D. L., and de Lange, T. (2008). 53BP1 promotes non-homologous end joining of telomeres by increasing chromatin mobility. Nature *456*, 524-528.

Dimri, G. P., Lee, X., Basile, G., Acosta, M., Scott, G., Roskelley, C., Medrano, E. E., Linskens, M., Rubelj, I., Pereira-Smith, O., Oeacicjem N, and Campisi, J. (1995). A biomarker that identifies senescent human cells in culture and in aging skin in vivo. Proc Natl Acad Sci USA *92*, 9363-9367.

Loayza, D., and de Lange, T. (2003). POT1 as a terminal transducer of TRF1 telomere length control. Nature *424*, 1013-1018.

Luo, G., Santoro, I. M., McDaniel, L. D., Nishijima, I., Mills, M., Youssoufian, H., Vogel, H., Schultz, R. A., and Bradley, A. (2000). Cancer predisposition caused by elevated mitotic recombination in Bloom mice. Nat Genet *26*, 424-429.

Silver, D. P., and Livingston, D. M. (2001). Self-excising retroviral vectors encoding the Cre recombinase overcome Cre-mediated cellular toxicity. Mol Cell *8*, 233-243.

Smogorzewska, A., van Steensel, B., Bianchi, A., Oelmann, S., Schaefer, M. R., Schnapp, G., and de Lange, T. (2000). Control of human telomere length by TRF1 and TRF2. Mol Cell Biol *20*, 1659-1668.

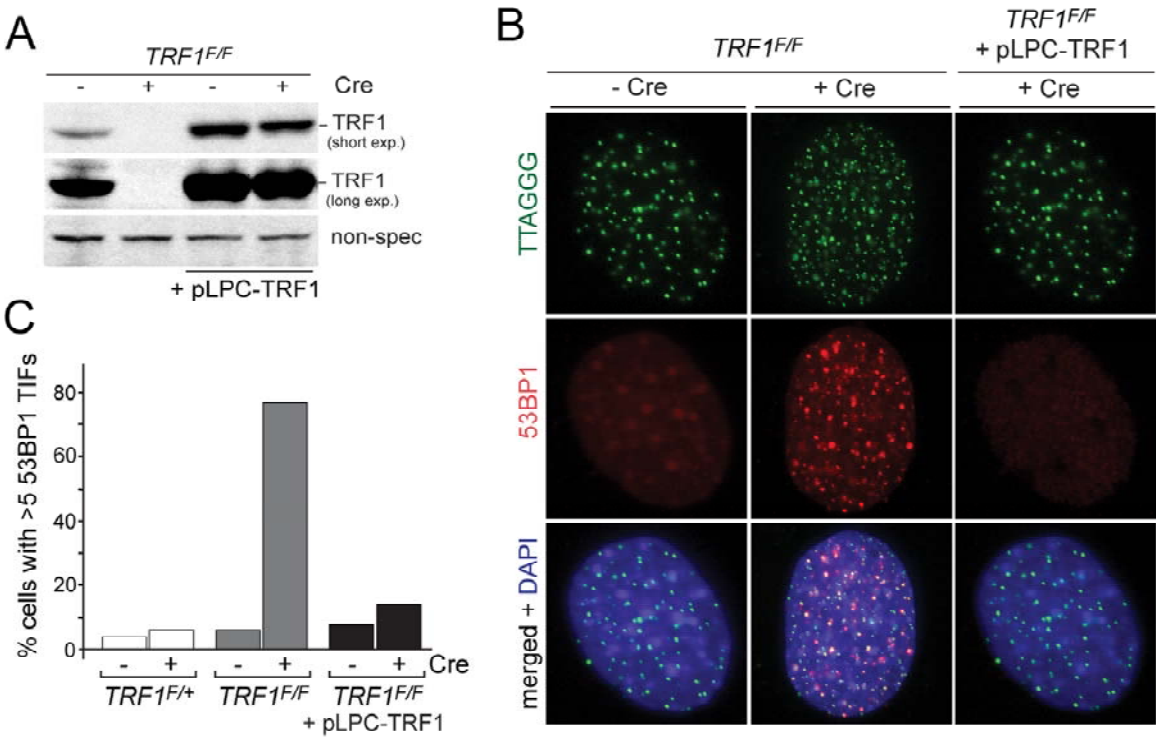

Figure S1. Exogenous TRF1 represses the phenotype of TRF1 deletion.
(A) Immunoblots for TRF1 in *TRF1$^{F/F}$* MEFs and *TRF1$^{F/F}$* MEFs expressing exogenous TRF1 (+pLPC Myc -TRF1) after H&R Cre infection or mock infection (-Cre).
(B) Cells of the indicated genotype and treatment were analyzed for TIF formation using FISH-IF with an antibody for 53BP1 (red) and a PNA probe (green) for telomeric DNA. DNA was counterstained with DAPI (blue).
(C) Quantification of the percentage of cells with 5 or more 53BP1 TIFs for the indicated treatment. Method as in (B).

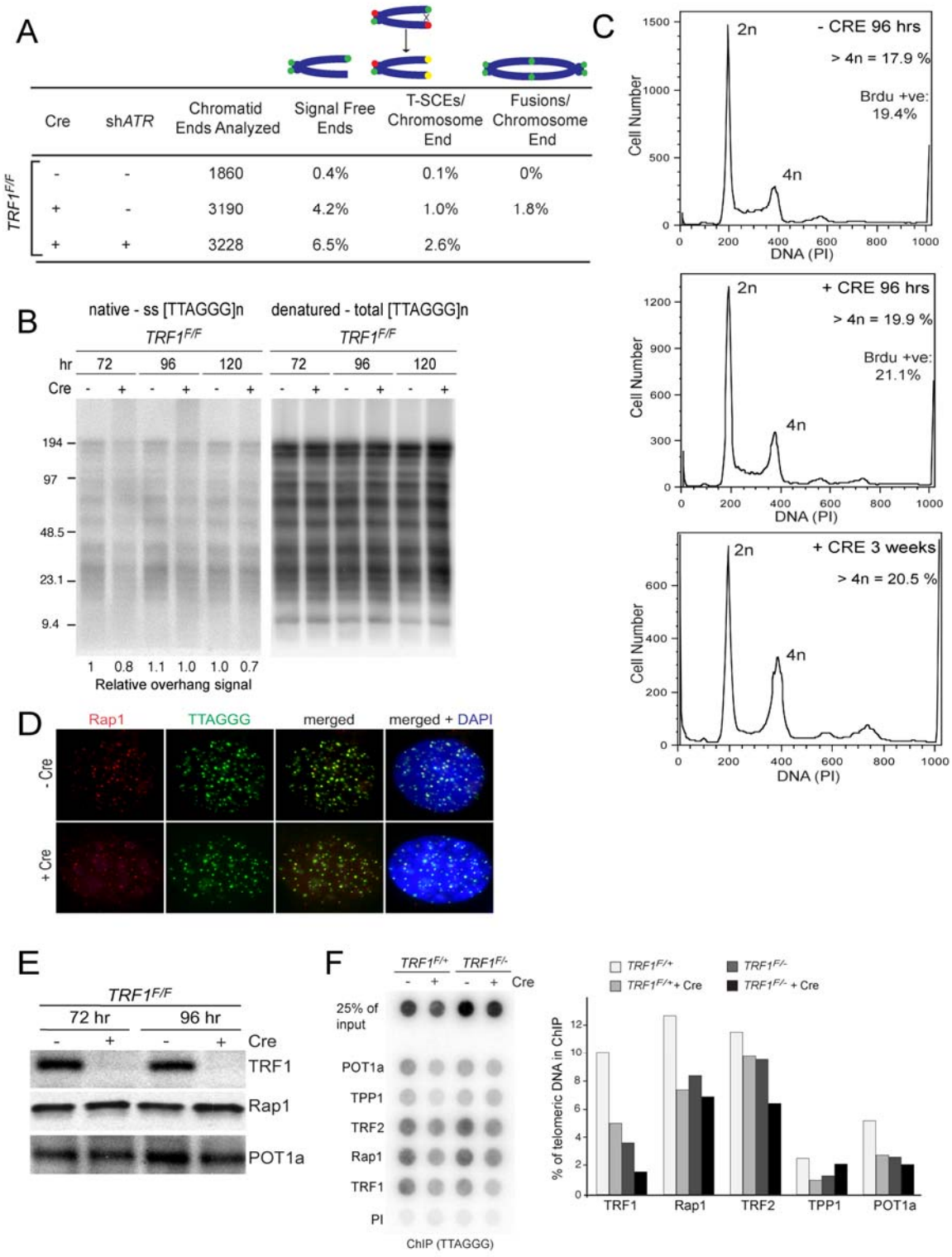

Figure S2. Effect of deletion of TRF1 from immortalized MEFs on telomere function and structure, cell cycle profiles, and other shelterin components.
(A) Frequencies of signal-free end, telomeric sister chromatid exchanges (T-SCEs) and telomere fusions in *TRF1*$^{F/F}$ MEFs with the indicated treatment and analyzed at day 4 after infection with Cre.

(B) In-gel detection of the structure of telomeric DNA from *TRF1*$^{F/F}$ MEFs at the indicated time points post Cre infection. The image on the left represents hybridization using a (CCCAAT)4 probe to detect the telomere overhang under native conditions. The image on the right represents total telomere hybridization signal obtained with the same probe after in situ denaturation of the DNA. The numbers on the bottom left represent the relative overhang signal.
(C) FACS profiles of *TRF1*$^{F/F}$ cells infected with pWZL-Cre or vector control analyzed at day 4 after infection. MEF lines infected with pWZL-Cre were also analyzed 3 weeks after infection. The percentage of cells >4n DNA content is noted within the FACS profile. Cells harvested at day 4 were pulsed with BrdU for 1 hr prior to harvesting to determine the S phase index. The percentage of BrdU positive cells is noted within the FACS profile.
(D) Immunofluorescence analysis for Rap1 at telomeres at day 4 post pWZL-Cre or vector control (-Cre) in *TRF1*$^{F/F}$ cells.
(E) Immunoblots to detect TRF1, Rap1 and POT1a at day 3 and day 4 after pWZL-Cre or vector control (-Cre) treatment of *TRF1*$^{F/F}$ cells.
(F) Telomeric DNA ChIP for shelterin. ChIPs with the indicated antibodies on *TRF1*$^{F/+}$ and *TRF1*$^{F/-}$ cells infected with pWZL-Cre or vector control and analyzed at day 4. Left: Dot blot of the precipitated telomeric DNA detected with a TTAGGG repeat probe. PI, pre-immune serum. Right: Bar graph of quantification of the % of TTAGGG repeats recovered in the IPs. The same results were obtained in a second, independent ChIP experiment.

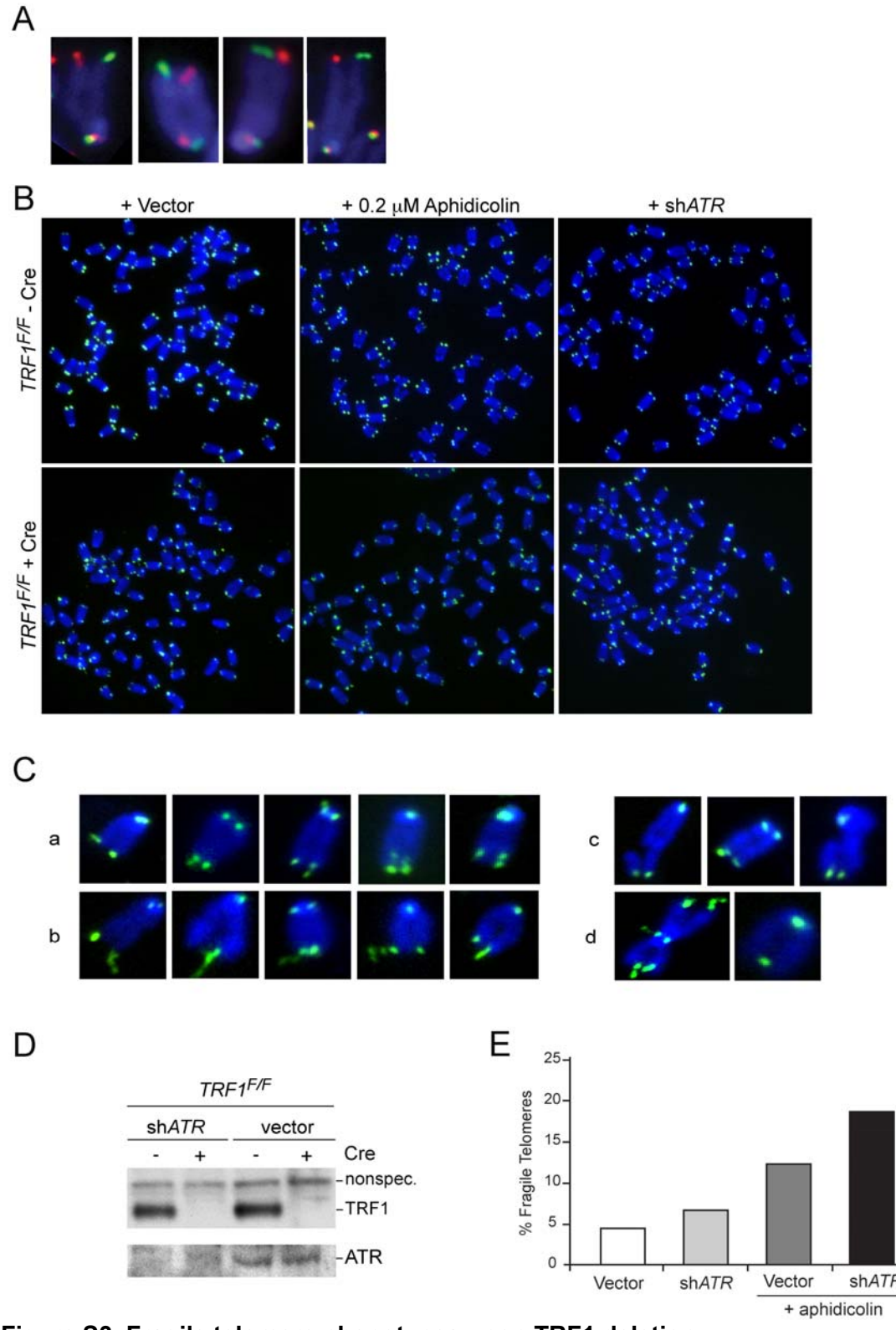

Figure S3. Fragile telomere phenotypes upon TRF1 deletion.
(A) Examples of fragile telomere phenotypes at both sister telomeres. TRF1$^{F/F}$ MEFs treated with H&R Cre and analyzed 4 days later using CO-FISH to visualize both sister telomeres. Among 471 fragile telomeres analyzed, 45% contained the parental G-strand

(B) Metaphase spreads of *TRF1*$^{F/F}$ MEFs with the indicated treatment and stained for telomeric DNA (FITC PNA probe in green) and DAPI (blue).
(C) Examples of fragile telomeres (a) and (b), chromosome breaks (c), and telomere fusions (d).
(D) Immunoblot showing TRF1 deletion and ATR knockdown in the cells used for the data in Fig. 2. The non-specific band serves as a loading control.
(E) Quantification of the percentage of fragile telomeres in TRF1-proficient cells following treatment with 0.2 μM aphidicolin and/ or ATR shRNA.

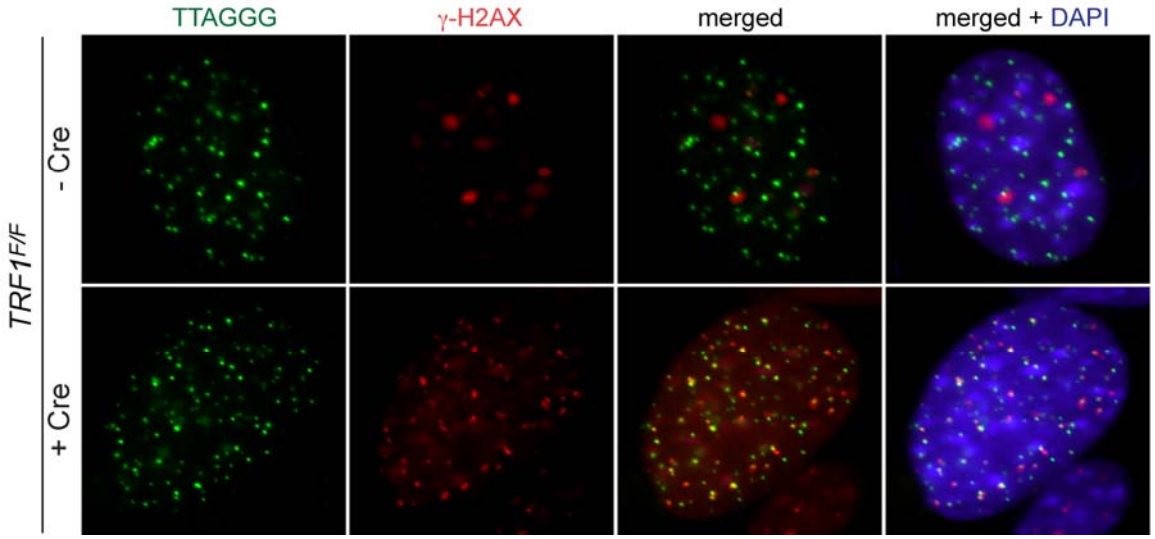

Figure S4. γ-H2AX at telomeres after deletion of TRF1.
TRF1$^{F/F}$ MEFs treated with H&R Cre or the empty vector were analyzed for FISH-IF by staining telomeres with a PNA probe (green) and γ-H2AX antibody (red). DNA was counterstained with DAPI (blue).

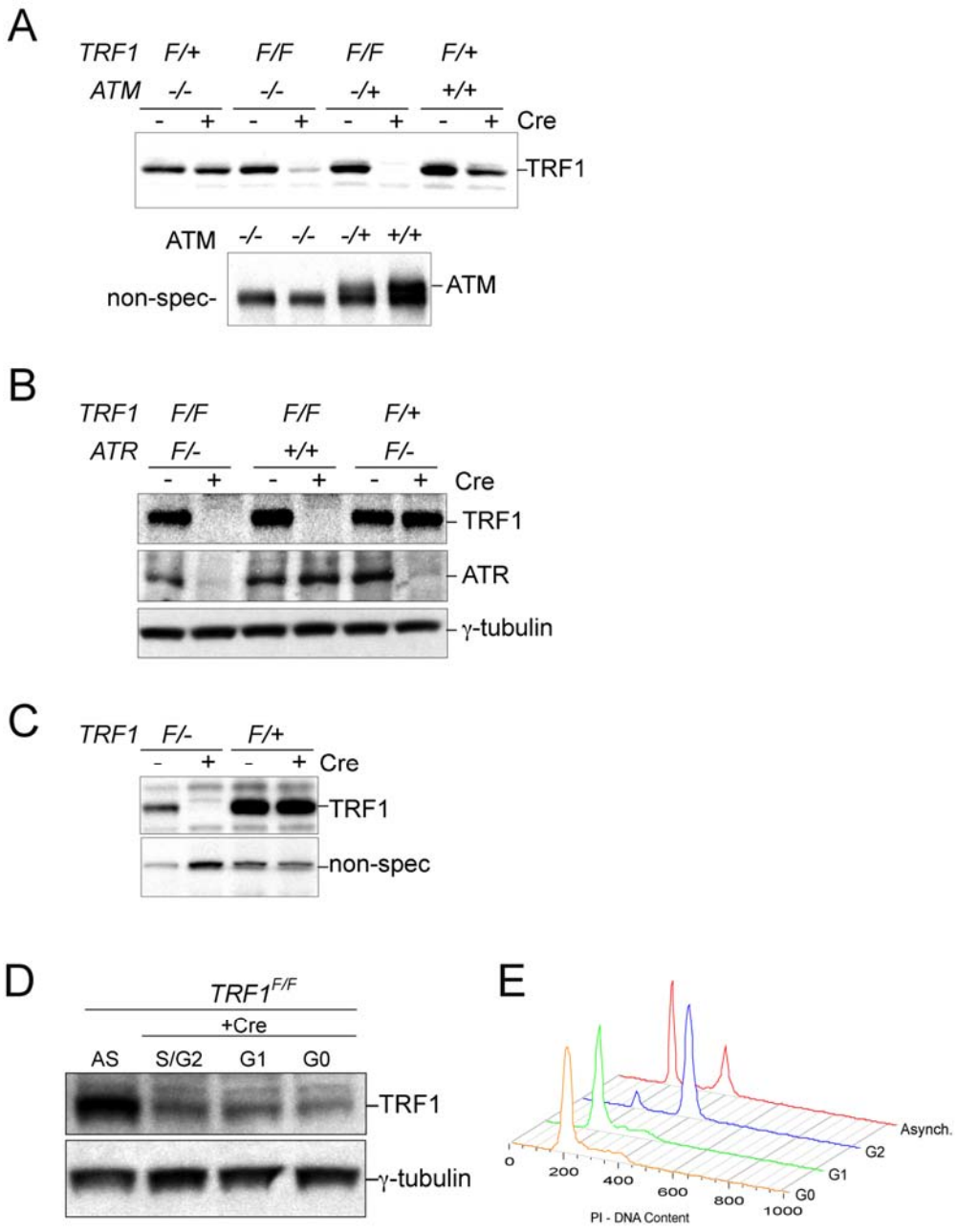

Figure S5. Immunoblots and FACS analysis relating to Figure 3.
(A) Immunoblots verifying ATM status and TRF1 deletion in the experiments shown in Fig. 3A and B.
(B) Immunoblots verifying ATR and TRF1 deletion in the experiments shown in Fig. 3A and B.
(C) Immunoblot showing TRF1 deletion from quiescent primary $TRF1^{F/-}$ cells used in Fig. 3A and B.
(D) Immunoblots showing partial deletion of TRF1 in the experiments in Fig. 3E.
(E) FACS profile (PI DNA content) of the samples used in Fig. 3E.

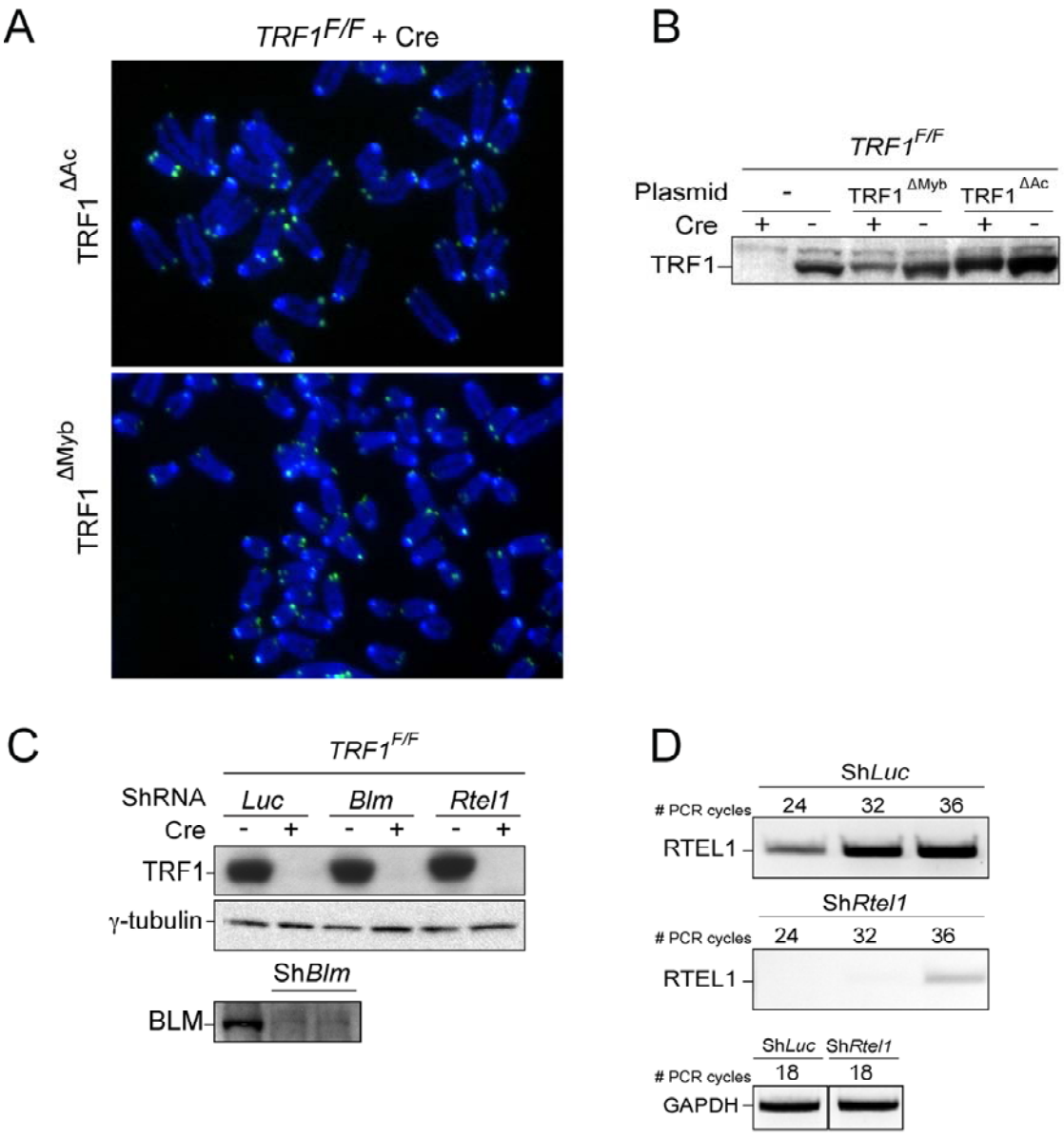

Figure S6. Metaphase spreads and Immunoblots relating to Figure 3.
(A) Metaphase spreads of *TRF1*$^{F/F}$ MEFs cells with the indicated treatment stained for telomeric DNA with a FITC PNA probe (green) and with DAPI (blue).
(B) Immunoblots of *TRF1*$^{F/F}$ MEFs expressing TRF1^{DAc} or TRF1^{DMyb} and treated with H&R Cre. The cells were analyzed at day 4 after Cre treatment.
(C) Immunoblot for TRF1 and *Blm* in *TRF1*$^{F/F}$ MEFs with indicated treatment at day 4 after Cre treatments.
(D) RT-PCR for *Rtel1*. RNA derived from TRF1 null cells infected with shRNA-encoding Lentivirus (*Rtel*1 and *Luc*) was processed to detect *Rtel* mRNA and *Gapdh* mRNA with RT-PCR.

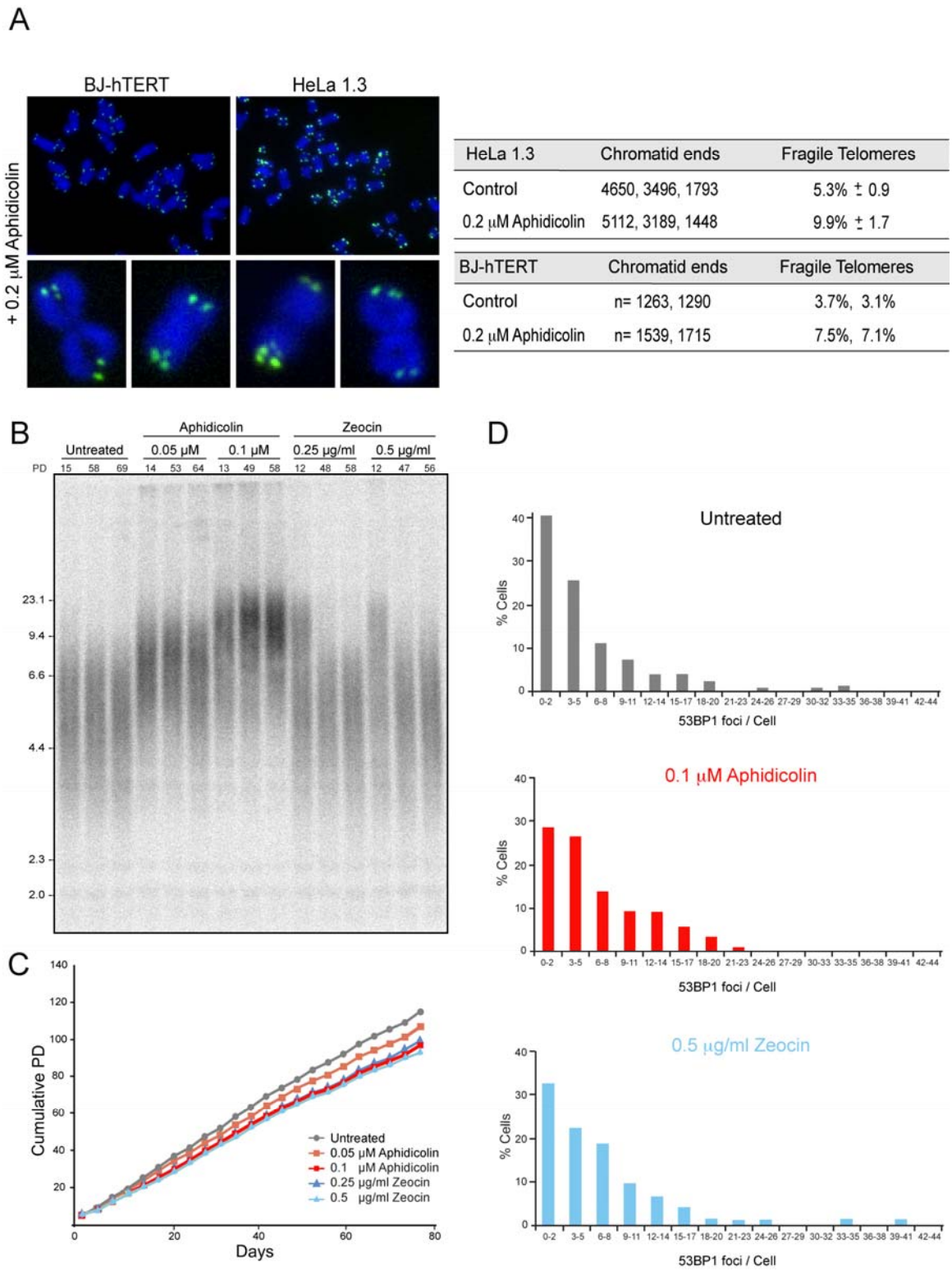

HeLa 1.3	Chromatid ends	Fragile Telomeres
Control	4650, 3496, 1793	5.3% ± 0.9
0.2 μM Aphidicolin	5112, 3189, 1448	9.9% ± 1.7

BJ-hTERT	Chromatid ends	Fragile Telomeres
Control	n= 1263, 1290	3.7%, 3.1%
0.2 μM Aphidicolin	n= 1539, 1715	7.5%, 7.1%

Figure S7. Fragile telomeres in human cells.
(A) Metaphase chromosomes of BJ-hTERT (human foreskin fibroblasts expressing ectopic telomerase) and Hela1.3 (a HeLa subclone with long telomeres) cells treated for 16hrs with 0.2 μM Aphidicolin and stained with a telomeric probe (FITC PNA probe in green) and DAPI (blue). The frequency of fragile telomeres in BJ-hTERT and Hela1.3

following treatment with 0.2 μM aphidicolin is represented in the tables. In the case of Hela 1.3, data are represented as mean +/- s.d. for triplicate experiments.
(B) Genomic blot of telomeric restriction fragments for HTC75 cells with the indicated treatments and concentrations. DNA at the indicated PD was analyzed by Southern blotting using a double-stranded TTAGGG repeat probe.
(C) The number of 53BP1 damage foci/cell in untreated HTC75 cells (upper panel), and in cells treated with 0.1 μM aphidicolin (middle panel) or 0.5 μg/ml Zeocin (lower panel).
(D) Graph representing growth curves of untreated HTC75 cells as well as HTC75 treated with aphidicolin (0.1 and 0.05 μM) and Zeocin (0.25 and 0.5 μg/ml).